AAEC/E228

AUSTRALIAN ATOMIC ENERGY COMMISSION

RESEARCH ESTABLISHMENT
LUCAS HEIGHTS

TWO-REGION CRITICAL EXPERIMENTS ON BeO-U235 REACTORS

by

A.P. MARKS

January 1972

ISBN 0 642 99461 7

AUSTRALIAN ATOMIC ENERGY COMMISSION

RESEARCH ESTABLISHMENT

LUCAS HEIGHTS

TWO-REGION CRITICAL EXPERIMENTS ON BeO-^{235}U REACTORS

by

A. P. MARKS

ABSTRACT

Reactor physics properties of a series of BeO-^{235}U assemblies were measured as part of a programme of development of a high temperature gas cooled reactor. Five such assemblies with moderator to fuel ratios ranging between 737 and 6539 to unity were placed between the core tanks of the Argonaut type reactor MOATA. Each assembly occupied a volume of one cubic foot and was subcritical in isolation; inserted into MOATA the assemblies formed a two-region critical system.

The report gives complete details of mechanical arrangements for the assembly components and for methods of emplacement in the reactor; it also discusses the limitations inherent in the availability of materials and the restricted volume for assembly location. Details are given of methods used for approach-to-critical and for calibration of control absorbers on each assembly.

Both theory and practical aspects of measurements made are covered in the text. Reference is made to differential neutron spectra by time-of-flight and chopper techniques, epithermal neutron spectra by activation of integral detectors, fission rate ratios by use of gas flow chambers, and reactivity measurements by long period sample oscillation. The methods employed are critically examined, and difficulties and disadvantages stated; in some cases alternative methods are compared.

An account is given of theoretical calculations complementing the measured values. The limited volume available prevented asymptotic spectra being attained, and the geometrical complexity led to serious difficulties in setting up the calculational model. The possibility of using discrepancies between experiment and calculation as a means of improving basic nuclear data and calculational methods was impaired by the compromises necessitated by the modelling difficulties. Nevertheless it is shown that experimental values could be reconciled with those calculated with the aid of some empirical adjustment, thus demonstrating internal consistency.

The work served to highlight the known need for simple geometry for the study of such assemblies, and provided valuable experience in evaluation of experimental and data analysis techniques.

National Library of Australia card number and ISBN 0 642 99461 7

The following descriptors have been selected from the INIS Thesaurus to describe the subject content of this report for information retrieval purposes. For further details please refer to IAEA–INIS–12 (INIS: Manual for Indexing) and IAEA–INIS–13 (INIS: Thesaurus) published in Vienna by the International Atomic Energy Agency.

ACTIVATION DETECTORS; ALUMINIUM; BERYLLIUM OXIDES; CALIBRATION; CONFIGURATION; CONTROL ROD WORTHS; CRITICAL MASS; CRITICALITY; CROSS SECTIONS; DATA; DATA PROCESSING; EPITHERMAL NEUTRONS; FISSION CHAMBERS; FISSION RATIO; FOILS; HIGHLY ENRICHED URANIUM; HTGR TYPE REACTORS; MOATA REACTOR; MODERATOR–FUEL RATIO; NEUTRON CHOPPERS; NEUTRON FLUX; NEUTRON SPECTRA; PILE OSCILLATION TECHNIQUES; REACTIVITY; REACTIVITY WORTHS; REACTOR CELLS; REACTOR FUELLING; REGULATING RODS; SHIM RODS; TEMPERATURE DEPENDENCE; TIME–OF–FLIGHT METHOD; URANIUM 235;

CONTENTS

(continued)

CONTENTS (continued)

1. INTRODUCTION

An account is given of reactor physics measurements made on assemblies of beryllium oxide with enriched uranium placed in the internal reflector of the Argonaut type reactor MOATA (Marks 1962). Each assembly consisted of a one-foot cube of BeO with added metal foils of highly enriched uranium.

The interest in beryllium oxide as a moderator arose from the A.A.E.C.'s feasibility study on a high temperature gas-cooled reactor which included a programme of measurements on BeO-moderated assemblies, together with a parallel development of calculational methods and associated library of basic nuclear data.

The measurements provided experimental check-points for comparison with calculations, but were far from being ideal, 'clean', measurements owing to lack of availability of materials and facilities. It was expected that subcritical assemblies with suitable materials ratios would provide neutron energy spectra of varying degrees of hardness. If they were large enough, the central spectra might be asymptotic and characteristic of a critical assembly of similar composition. Even if asymptotic spectra were not obtained, it was considered that the calculational methods would allow prediction of the actual measured properties, and thus enable necessary adjustments to be made to data and methods.

An initial series of conventional exponential experiments (Duerden et al. 1964) gave flux distribution and integral spectrum data. These exponentials could not provide flux levels high enough to enable measurement of further parameters such as differential spectra or reactivity effects of perturbations by various materials. To fill this gap further series of assemblies were studied as part of a critical system by inserting them into the internal reflector of MOATA. They were of necessity smaller than the exponential experiments, solely because of the limited volume available in the reactor.

This report gives comprehensive details of the assemblies studied in the latter part of the experimental programme, the methods used to obtain experimental parameters, and the results obtained. An account is given of calculations in support of the measurements, and comparisons between experiment and theory. Finally it is shown that although the complex geometry of the assembly necessitated some empirical adjustments in the calculations, there was a reasonable measure of agreement of general validity, between measurement and calculations.

2. ASSEMBLY DETAILS

Each of the five assemblies was built in an aluminium experiment container using BeO blocks, ^{235}U foils, and aluminium sheets which are described in more detail below.

2.1 Experiment Container

The experiment container (Figure 1) was a cubical box, twelve inches on edge internally, constructed of quarter-inch aluminium plate, with a removable lid of similar material. Lifting lugs were provided. Two opposite side faces had holes into which could be fitted either blanking discs, a thin aluminium window, a one-inch internal diameter tube extending across the box, or a two-inch internal diameter tube.

These alternative arrangements provided for four types of loading, each utilised for particular measurements on the BeO-^{235}U assemblies placed in the box. The alternatives were:

(a) Full box, which was arranged to exclude, as far as possible, all voids and extraneous materials and to include a full cubic foot of BeO-^{235}U.

(b) Chopper channel, in which an access hole 6 inches long, 1 inch high and 1.140 inches wide, was provided between one face of the box and the centre of the assembly.

(c) 2-inch through tube, and

(d) 1-inch through tube, in both cases arranged to extend from one face to the opposite face.

The assembly materials were placed around the tubes with a minimum practical void volume. These tubes enabled reactivity samples and integral detectors to be placed within the assembly and be conveniently removed through the reactor shielding.

The mass of aluminium in each of the box components is listed in Table 1.

TABLE 1

ALUMINIUM EXPERIMENT CONTAINER--COMPONENT WEIGHTS

Component	Weight (grams)
Box plus lid	9497
Blanking plate	44
Aluminium window assembly	33
2-inch tube (within box)	211
1-inch tube (within box)	116

2.2 BeO Blocks

The beryllia was in blocks or tiles from two different sources. The 6 x 6 x 1 inch tiles, density 2.86 g cm^{-3}, were originally supplied by Brush Beryllium Company, while smaller blocks, as detailed below, were fabricated by the A.A.E.C. Materials Division and had a density of about 2.90 g cm^{-3}. These blocks were supplied from hot pressed UOX and NGK BeO powders, annealed at 1150°C, machined, and finally re-annealed at 800°C. Figure 2 shows details of the various BeO blocks and Figure 1 also shows how they were built up into the one-foot cube for the full box, chopper channel, and two-inch tube cases. The one-inch tube arrangement was similar to that for the two-inch tube, except that Type D blocks were substituted for Type B, and Type F blocks were used on the central layer adjacent to the tube on both sides.

It was impracticable to assign fixed locations to individual blocks throughout the series of assemblies. Thus to calculate material ratios the mean densities of the two series of blocks were used to calculate masses from theoretical volumes. These quantities are given in Table 2.

Table 3 shows the combination of blocks used in each assembly, and gives total weights of beryllia. From Assembly 3 onwards a consistent arrangement of blocks was employed; some variations occurred before the most convenient pattern was found. Eleven one-inch layers of beryllia were used in each assembly.

2.3 Uranium Foils

Enriched uranium foils, 2 x 4 x 0.002 inches, from two separate sources were used (93 percent ^{235}U of U.K. origin, and 89.8 percent ^{235}U of U.S. origin). Assays are given in Table 4. No cladding or coating was used on the foils.

In Assembly 1, the foils were laid on each BeO layer with no method of adhesion or other positive location. In all other assemblies the foils were located on one-foot square, 1/16 inch thick aluminium sheets, by using minimal spots of contact adhesive on two corners of each foil.

Each assembly had ten layers of foils and the numbers of foils per layer and other details are given in Table 5. In some assemblies, foils had to be omitted from the layers immediately above and below the centre of the experiment container to make way for the two-inch and one-inch tubes; the corresponding values are given in Table 5.

TABLE 2

BeO BLOCKS-VOLUMES AND WEIGHTS (See Figure 2)

Block Type	Origin	Density (g cm^{-3})	Volume (cm^3)	Weight (g)	Dimensions (inches)
A	A.A.E.C.	2.90	147.48	427.70	3 x 3 x 1
B	A.A.E.C.	2.90	127.62	370.10	Notched – See Figure 2
C	A.A.E.C.	2.90	94.48	274.00	3 x 1 $\frac{59}{64}$ x 1
D	A.A.E.C.	2.90	147.10	426.59	3 x 3 x 1 with rebate
E	Brush	2.86	589.94	1687.22	6 x 6 x 1
F	A.A.E.C.	2.90	23.81	69.06	3 x 1 x $\frac{31}{64}$
G	A.A.E.C.	2.90	37.36	108.35	2 x 1.14 x 1

TABLE 3

USE OF BeO BLOCKS

Assembly	Arrangement	Nos. of Blocks of Types							Total Weight g
		A 427.70g	B 370.19g	C 274.00g	D 426.59g	E 1687.22g	F 69.06g	G 108.35g	
1	Full box	–	–	–	–	44	–	–	74238
	Chopper Channel	16	–	8	–	40	8	3	77402
	2 inch Tube	24	16	8	–	32	–	–	72369
2	Full box	–	–	–	–	44	–	–	74238
	Chopper Channel	8	–	8	–	40	8	3	73980
	2 inch Tube	24	16	8	–	32	–	–	72369
3	Full box	8	–	8	–	40	8	6	74305
	Chopper Channel	8	–	8	–	40	8	3	73980
	2 inch Tube	24	16	8	–	32	–	–	72369
	1 inch Tube	24	–	8	16	32	8	–	73826
4	Full box	8	–	8	–	40	8	6	74305
	Chopper Channel	8	–	8	–	40	8	3	73980
	2 inch Tube	24	16	8	–	32	–	–	72369
	1 inch Tube	24	–	8	16	32	8	–	73826
5	Full box	8	–	8	–	40	8	6	74305
	Chopper Channel	8	–	8	–	40	8	3	73980
	2 inch Tube	24	16	8	–	32	–	–	72369
	1 inch Tube	24	–	8	16	32	8	–	73826

TABLE 4

ASSAY OF URANIUM FOILS

(Values are quoted in atom-percent)

Isotope	U.K. Batch FF8	U.S.A. Batch FF23
^{234}U	1.279	1.049
^{235}U	92.72	89.76
^{236}U	0.254	3.01
^{238}U	5.75	6.19

TABLE 5

URANIUM FOILS

Assembly	Arrangement	No. of Foils per Layer		Totals	
		Central Layers	Other Layers	No. of Foils	^{235}U Mass(g)
1	Full box	2	2	20	97.01
	Chopper Channel	2	2	20	97.01
	2 inch Tube	2	2	20	97.01
2	Full box	3	3	30	145.37
	Chopper Channel	3	3	30	145.37
	2 inch Tube	2	3	28	135.47
3	Full box	6	6	60	290.56
	Chopper Channel	6	6	60	290.56
	2 inch Tube	4	6	56	271.70
	1 inch Tube	4	6	56	271.70
4	Full box	12	12	120	565.43
	Chopper Channel	12	12	120	565.43
	2 inch Tube	6	12	108	509.26
	1 inch Tube	6	12	108	509.26
5*	Full box	18	18	180	859.94
	Chopper Channel	18	18	180	859.94
	2 inch Tube	12	18	168	804.30
	1 inch Tube	12	18	168	804.30

* Note that Assemblies 1 to 4 inclusive used only foils of Batch FF23, 89.8 percent ^{235}U. In Assembly 5, foils of Batch FF8, 93 percent ^{235}U were used in the two lowest and two topmost layers, Batch FF23 foils occupying the central six layers. Masses involved were respectively 351.17 g ^{235}U (FF8) and 508.77 g ^{235}U (FF23).

2.4 Materials Ratios

It is clear from the above details that there was a certain non-uniformity of distribution of material in the assemblies. In particular, the tube arrangements necessitated the use of small additional amounts of aluminium sheet to allow the shaped BeO blocks to fit around the tubes (see Table 6). Appendix 1 gives complete details of the composition of each arrangement.

TABLE 6

ALUMINIUM USED IN ASSEMBLIES

Assembly	Arrangement	Aluminium Components			Total Mass (g)
		1/16 inch Sheets*	Shims	Tube	
1	Full box	–	–	–	0
	Chopper Channel	–	9.5 g	–	9.5
	2 inch Tube	8	430.2 g	211 g	3826.9
2	Full box	13	–	–	5176.7
	Chopper Channel	12	9.5 g	–	4788.0
	2 inch Tube	12 +	143.4 g	211 g	5021.5
3	Full box	12	–	–	4778.5
	Chopper Channel	12	9.5 g	–	4788.0
	2 inch Tube	12 +	143.4 g	211 g	5021.5
	1 inch Tube	12 +	143.4 g	116 g	4926.5
4	Full box	12	–	–	4778.5
	Chopper Channel	12	9.5 g	–	4788.0
	2 inch Tube	12 +	143.4 g	211 g	5021.5
	1 inch Tube	12 +	143.4 g	116 g	4926.5
5	Full box	12	–	–	4778.5
	Chopper Channel	12	9.5 g	–	4788.0
	2 inch Tube	12 +	143.4 g	211 g	5021.5
	1 inch Tube	12 +	143.4 g	116 g	4926.5

* Each 1/16 inch sheet, 12 inches square, weighed 398.21 g

\+ Reduced by 111.4 g for each of two central layers, where two 4½ inch wide sheets were used to clear the tube

From this information atom ratios of BeO : Al : ^{235}U were computed. Such ratios, however, clearly depend on the volume over which the materials were homogenised. At first, the calculation was carried out for the complete contents of the experiment container for each arrangement, disregarding only the walls of the container itself. In addition, values were derived for an 'ideal-cell'. This ideal cell was considered to consist of the BeO and Al sheet associated with one uranium foil in each assembly. Thus the quantities of BeO and Al in one layer were divided by the number of foils per layer, to arrive at the quantities in the ideal cell. The foil weight used was averaged over the total weight of ^{235}U used in the full box arrangement for the particular assembly. Atom densities were found from the volume of the layer associated with each foil.

Table 7 gives the overall values, and Table 8 gives the ideal cell values. It must be emphasised that no unique atom ratio can be quoted for a given assembly, as the ratio varies with the particular arrangement used.

2.5 Errors

Ratios given in Tables 7 and 8 are subject to some uncertainties, due to both the method of calculating BeO masses and the precision with which Al and ^{235}U quantities were known. These uncertainties have not been studied comprehensively but from known tolerances for BeO dimensions and other material values, the ratios could be in error by from one-half to one percent.

TABLE 7

MATERIALS AND MATERIAL RATIOS

Assembly	Arrangement	Total Material Masses (g)			Atom Ratios		
		BeO	Al	^{235}U	BeO	Al	^{235}U
1	Full box	74238	0	97.01	7191	0	1
	Chopper Channel	77402	10	97.01	7498	0.90	1
	2 inch Tube	72369	3827	97.01	7010	344	1
2	Full box	74238	5177	145.37	4799	310	1
	Chopper Channel	73980	4788	145.37	4782	287	1
	2 inch Tube	72369	5022	135.47	5020	323	1
3	Full box	74305	4779	290.56	2403	143	1
	Chopper Channel	73980	4788	290.56	2393	144	1
	2 inch Tube	72369	5022	271.70	2503	161	1
	1 inch Tube	73826	4927	271.70	2553	158	1
4	Full box	74305	4779	565.43	1235	74	1
	Chopper Channel	73980	4788	565.43	1229	74	1
	2 inch Tube	72369	5022	509.26	1335	86	1
	1 inch Tube	73826	4927	509.26	1362	84	1
5	Full box	74305	4779	859.94	812	48	1
	Chopper Channel	73980	4788	859.94	808	49	1
	2 inch Tube	72369	5022	804.30	846	54	1
	1 inch Tube	73826	4927	804.30	863	53	1

The atom ratios have been calculated using atomic weights of 25.0122 for BeO, 26.9815 for Al, and 235.0439 for ^{235}U.

3. REACTOR ARRANGEMENTS

The central region of MOATA was modified to enable the one-foot cube experiment container to be inserted into the volume between the two core tanks (see Figure 3). The graphite internal reflector, which extends for 18 inches between the core tanks was modified so that a column of graphite approximately 12½ inches square in section, and 4 feet long, could be removed. A graphite prism, about 18 inches high, then formed the support for the experiment container, and the latter, when in position, was covered by a further 18 inches of graphite. This was provided with a number of removable stringers, which gave access from the core top face down to the assembly box.

A hole of at least 2 inches square section was provided through the centre of the reactor (and hence through the experiment container) parallel to the core tanks; access was available from both north and south sides of the reactor, through the north and south irradiation cavities.

The south hole was used for differential spectrum measurements using the time-of-flight spectrometer (Tattersall 1967a, 1967b) and the chopper rotor itself was installed on the inside of the south cavity closure door. All other measurements which required access to the centre of the assembly box used the northern hole to insert fission counters, activation detectors, reactivity oscillator, etc., into assemblies.

TABLE 8

IDEAL SINGLE CELL ATOM RATIOS AND DENSITIES

Assembly	No. of Foils per Layer	Cell Volume (cm^3)	Masses per cell (g)			Densities (g cm^{-3})			Atom Densities (10^{24} cm^{-3})			Atom Ratios		
			BeO	Al	^{235}U	BeO	Al	^{235}U	BeO	Al	^{235}U	BeO	Al	^{235}U
1	2	1182.2	3374	0.0	4.85	2.854	0.0	4.103×10^{-3}	6.872×10^{-2}	0.0	1.051×10^{-5}	6539	0	1
2	3	838.5	2250	133.0	4.85	2.683	0.1586	5.784×10^{-3}	6.461×10^{-2}	3.540×10^{-3}	1.482×10^{-5}	4360	239	1
3	6	419.3	1125	66.4	4.84	2.683	0.1584	11.54×10^{-3}	6.461×10^{-2}	3.535×10^{-3}	2.957×10^{-5}	2185	120	1
4	12	209.6	562	33.2	4.71	2.681	0.1584	22.47×10^{-3}	6.456×10^{-2}	3.535×10^{-3}	5.757×10^{-5}	1121	61	1
5	18	139.8	375	22.1	4.78	2.682	0.1581	34.19×10^{-3}	6.458×10^{-2}	3.529×10^{-3}	8.759×10^{-5}	737	40	1

$$\text{Cell volume}^{*} = \frac{2515.5}{\text{No. of foils per layer}} \ cm^3$$

$$\text{BeO per cell} = \frac{6748.9}{\text{No. of foils per layer}} \ g$$

$$\text{Al per cell} = \frac{398.21}{\text{No. of foils per layer}} \ g$$

$$^{235}U \text{ per cell} = \frac{\text{Total mass of } ^{235}U}{\text{No. of foils}}$$

$$\frac{\text{Avogadro's number}}{\text{Atomic weight}} = 0.2408 \times 10^{23} \text{ for BeO}$$

$$= 0.2232 \times 10^{23} \text{ for Al}$$

$$= 0.0256 \times 10^{23} \text{ for } ^{235}U$$

* Assembly 1 only: 2364.5/No. of foils

4. INITIAL LOADING AND CRITICAL MASS

4.1 Loading and Approach-to-Critical

The experiment container, loaded with the appropriate amounts of BeO and ^{235}U, was installed in the graphite internal reflector of MOATA with graphite above, as described in Section 3. Owing to some uncertainty about the possible critical mass of the complete system comprising reactor fuel and experiment container, all reactor fuel was removed before installation of the experiment container in some assemblies; in other cases, a proportion of the reactor fuel was allowed to remain in the core tanks. As confidence was gained in the trend of critical mass with increased ^{235}U loadings in the experiment container, it was found unnecessary to remove all reactor fuel before a loading change.

In addition to the installed reactor ionisation chambers, on the top face of the reflector graphite additional flux-measuring devices were used for the approach-to-critical. These were pulse fission chambers or BF_3 proportional counters, with conventional 1430A Main and Head Amplifiers and A.A.E.C. Type 2 Scalers. These additional counters were installed in reactor facilities IR-6, ER-5 and the Vertical Cavity (see Figure 3). IR-6 is a 2-inch diameter hole in the graphite immediately above the centre of the experiment container, and thus near the mid-point of the reactor and mid-way between the two core tanks. ER-5 is a 2-inch diameter hole in the graphite adjacent to the southern end of the west core tank. The Vertical Cavity lies above the graphite thermal column at the east end of the reactor and a hole in this cavity was utilised to place the counting tube immediately on top of the thermal column.

The approach-to-critical, following loading of the experiment container, proceeded normally.

Owing to the particular geometry of MOATA, and the possible locations of counters, linearity only appeared to exist when the reactor was very close to critical, (e.g. about 5.10^{-3} $\delta k/k$). Nevertheless, safety reasons alone made it difficult to adopt a less protracted method of loading a new and untried core configuration.

Each additional loading of reactor fuel was made as symmetrically as the allowable quantity permitted. Thus equivalent fuel masses were loaded in similar locations in both core tanks whenever possible. In all assemblies, full 12-plate fuel elements were used in core tank locations B, C, D, E, H, I, J and K (Figure 3). In the remaining four corner locations A, F, G and L, similar numbers of fuel plates were used when the loading permitted.

4.2 Criticality

The final loading for criticality was arranged to make the reactor critical with as little control absorber insertion as possible, that is, the reactor could be taken critical with both safety rods and the shim-safety rod fully withdrawn, and the regulating rod withdrawn at least some part of its travel.

The actual critical mass was then estimated from extrapolations of the final inverse count-rate data for the case where all control rods were withdrawn. Table 9 shows critical masses obtained in this way (marked 'Subcritical'), and Figure 4 gives a typical extrapolation.

TABLE 9

CRITICAL MASSES

Assembly	Extrapolated Critical Mass (g ^{235}U total)		Mass of ^{235}U in Core Tanks (grams)
	Subcritical	Critical	
1	3007 – 3010	3001	2904
2	3000 – 3005	3002	2857
3	2970 – 2972	2974	2683
4	3044 – 3052	3032	2467
5	3197 – 3198 *	3187	2327

* Measured with IR-6 and ER-5 stringers removed, giving an estimated additional mass of 5 grams ^{235}U that is estimated critical mass compared with previous assemblies is 3192 – 3193 grams.

Criticality having been attained, further reactor fuel was required to give some operational flexibility. For example, insertion of experimental equipment in the reactor, or removal of graphite for access to the experiment container, caused loss of reactivity, and more fuel was necessary to compensate. Fuel was added in small increments of one-half or one full-load plate at a time. In each case, the (excess) reactivity of the reactor was determined by period measurements, and a series of values found relating fuel loading to reactivity. These values were then extrapolated back to obtain a zero-reactivity fuel loading, corresponding to the critical mass (marked 'Critical' in Table 9).

Period (or doubling-time) measurements were converted to reactivity values by using an inhour curve calculated for ^{235}U delayed neutron groups only. Some contribution from beryllium photoneutrons, resulting from fission product gamma-interactions from previously-irradiated uranium foils existed but the effect has been shown to be small (W.J. Turner, AAEC private communication, has found photoneutron fractions to be less than 1 percent of delayed neutron fraction with a beryllia block only in position) and in any case uncertain. No account was taken of it in the present work.

Figure 5 shows the trend of critical mass with assembly composition. Details of control rod calibrations follow.

5. CONTROL ABSORBER CALIBRATIONS

Information on control absorber worth for each reactor configuration was required both for safety reasons and for calibration of other measurements in each assembly.

5.1 Differential Worth Measurements

The process of loading fuel in the approach-to-critical gave rise to measurements of shim-safety and regulating rod reactivity worth in terms of equivalent fissile mass. After criticality had been attained, the incremental reactivity worth of the safety and regulating rods as a function of position was measured.

5.1.1 Shim rod

The worth of appropriate movements of the shim rod was measured using the period technique. In most cases, the period produced was confined to a range long enough for accuracy, yet short enough to avoid reactor drifts, that is, between about 30 and 180 seconds. During every measurement a record of core temperature was kept using a platinum resistance thermometer – potentiometric recorder combination with expanded scale. The thermometer itself was immediately beneath the core tanks, in the six-inch entry line for the primary water. The reactor doubling-time was measured in each case.

The raw doubling-time data were examined for existence of an asymptotic value and a mean value was found and converted into period and thence reactivity. The conversion into reactivity was made using the tables given by Keepin (1965) for the case of ^{235}U. As mentioned in Section 4, no account was taken of delayed neutron groups associated with fission-product photon reactions with beryllium. Critical settings were however, established at flux levels significantly above the photo-neutron source level.

These reactivity values were then taken in conjunction with the rod movement concerned, to produce a value of rod sensitivity for the mean position of the rod during the measurement. The collection of sensitivities found in this way for all reactor conditions for each assembly was then plotted, and a subjective assessment made of the consistency of the results. A typical plot of sensitivity is shown in Figure 6. Points showing gross departure from the general trend were omitted for numerical integration of the curve using essentially the trapezoidal rule for unequal abscissa differences. A curve of integral rod worth resulted. The integral curve was then used to find a smoothed sensitivity value for the next step, which involved the use of subcritical multiplication methods to extend the integral and sensitivity curves to the lower parts of the rod travel.

Both the fuel loading and the reactivity of the entire reactor varied during work on each assembly. Fuel was added initially to provide a working margin, and then as various experiments were loaded and unloaded. Thus the critical setting of the shim rod, in particular, varied in most cases over a large fraction of its span ot 0 to 300°. This enabled period measurements to be performed over a wide range of mean shim rod settings for each assembly.

In the subcritical multiplication method, a rod sensitivity measured by the period technique was used to calibrate a small movement of the rod below critical, it being assumed that the sensitivity was not markedly different immediately above and below a critical setting. A number of flux-measuring channels were then set up, and the count-rates noted for the just-subcritical condition. Use of the expression

$$\text{count-rate} = A/(1 - k_o) = A/\Delta k_o \quad ,$$

where A is a constant, and $1 - k_o$ the reactivity below critical, enabled the constant A to be evaluated for each channel. The rod was then inserted further, and the new count-rate noted when it became steady. The above expression was then used for calculation of appropriate values of $1 - k_1$, or Δk_1, and so on. Subcritical sensitivities found in this way were combined with period-derived data to extend the integral-worth curve down to 0°.

The above methods, though applicable to both shim and regulating rods, were mainly used for the shim rod. Figure 7 shows the integral worth curves obtained for assemblies 1 to 5.

5.1.2 Regulating rod

Use of the above methods to determine integral worth of the regulating rod was hampered by its small worth (10^{-3} $\delta k/k$). To find sensitivity values closely spaced along the range of the rod, lengthy reactor periods would have to be produced, leading to problems with reactor drift, in addition to the time needed to conduct the measurement. In one case (assembly 3) the period technique was used, in another (assembly 2) the oscillator method. In the latter the flux modulation amplitude resulting from small amplitude sinusoidal oscillations of the rod was measured at various points in its range. The reactor was assumed to be a linear system and the zero power transfer function applicable. The values of flux amplitude, recorded simultaneously with those of rod amplitude, then gave relative sensitivities enabling a curve to be drawn which provided the correct shape for integral worth as a function of rod position. The curve was normalised by a period measurement of total rod worth (from 0° to 300°).

Practical problems associated with this technique arose from the compromise between measurable flux amplitudes, and attainable rod amplitudes, bearing in mind limitations on speed of rod movement. This led to some difficulty in accurately measuring flux amplitudes for positions near the ends of the rod travel.

When the rod oscillator method was used, the reactor automatic power controller was modified to produce the sinusoidal rod motion. The modification involved replacement of the normal power error signal by a regular locally generated sine wave signal. Rod amplitude was measured on a chart recorder connected to the rod position feedback potentiometer, while the flux amplitude was estimated manually from a noisy signal on the expanded scale linear power recorder attached to the Keithley 411 micro-microammeter. Results of this measurement, in integral form, are given in Figure 8.

A variation of the rod oscillator method was tested on assembly 2. The Pace 231R analogue computer was linked by telephone lines to MOATA, and used to produce the low-frequency (0.05 Hz) sine-wave driving the regulating rod. The flux signal was then returned via the telephone lines to the computer, where a correlation method was used to integrate the flux and improve the signal-to-noise ratio. This set of measurements was not wholly successful, probably as a result of noise pick-up along unshielded lines. The method could be improved by attention to this problem.

5.2 Total Worth Measurements

The total worth of shim and regulating rods above were obtained from the differential worths by integrating sensitivity values. Total worths for the two safety rods were also measured by subcritical multiplication (Section 5.1) and on one occasion (assembly 5) by integral counting.

Flux-measuring detectors used for subcritical multiplication were located in the IR-6, ER-5, and vertical cavity facilities. Results from each detector channel were often somewhat dissimilar, presumably because of variations in neutron spatial behaviour away from critical. Since total worth figures for safety rods are required mainly for safety reasons, high accuracy is not normally required, and in this case a simple mean was taken between the three values measured on each occasion.

The integral counting method involves recording the steady count-rate on a flux measuring channel with the reactor critical and at a level power, followed by accumulation of counts on the same channel after the rapid insertion of the rod concerned. The theory of the method (Hogan 1960, Keepin 1965) involves delayed neutron fractions and effectiveness. Thus the results obtained are influenced by any delayed photoneutron contribution which may be present. Counting was continued until the residual count-rate was small, after which an estimate of the residual period was made using the linear power recorder trace. The estimate enabled a correction to be made for the 'counts to infinity'. Again delayed photoneutrons were ignored in analysing the results.

The expression used for reactivity by the integral count technique is

$$-\rho = (N(0)/n(0)) \sum_i (\beta i/\lambda i) \qquad \text{(units of } \delta k/k),$$

where $N(0)$ = count-rate at initial power level

$n(0) = \int_0^\infty N(t)dt$ = integrated counts from the time of absorber insertion.

$n(0)$ may be corrected from observed total counts $n(t)$, residual count-rate $n(t)$ and period τ as $n(0) = n(t) + \tau N(t)$, where it is desirable that $\tau N(t) << n(t)$.

The value used for $\sum_i (\beta i/\lambda i)$ for ^{235}U was 0.0847.

Table 10 summarises total rod worths for the five reactor configurations.

TABLE 10

TOTAL ROD WORTHS

(Values in 10^{-2} $\delta k/k$)

Assembly No.	Shim Rod	Regulating Rod	Safety Rod No. 1	Safety Rod No. 2
1	0.465	0.110	0.354	0.586
2	0.470	0.112	0.318, 0.351 *	0.409, 0.491 *
3	0.449	0.090	0.335	0.362
4	0.408	0.082	0.238	0.254
5	0.384	0.078	0.302 +	0.376 +

* No graphite in north cavity

+ Integral counts method

Although the absorbers on both safety rods and on the shim rod are physically similar, Table 10 shows differences in total worths on any one reactor configuration. A lack of symmetry in the flux shape across the core is the cause of these differences (Wall, private communication 1969). Since $\delta k/k \sim \phi^2_{local}$, the results suggest that ϕ_{local} varies from one rod position to another. Asymmetry in fuel loading and in leakage are causes of these variations.

A further feature is a general decrease in total worths relative to assemblies themselves containing greater fuel loadings, an effect which may be qualitatively explained in terms of decreased reactor fuel loading. Elements A, F, G and L, which are near the control absorbers, suffer the reduction in loading when more fuel goes to the assembly and less to the core tanks.

5.3 Temperature Coefficient of Reactivity

In most measurements described above, there was little dependence on temperature effects, provided that temperature changed by less than about one degree Fahrenheit during a measurement. However, this was not so for reactivity values used to extrapolate back for critical mass (see Section 4.2). In the latter case, the reactor was very close to critical, and temperature changes of the order of one degree Fahrenheit gave reactivity effects comparable to the reactivity of the reactor. Thus variations of temperatures during the loading above critical gave rise to some uncertainty in reactivity/fuel mass values.

Only for assembly 4 was a formal measurement of temperature coefficient made. In this case, the reactor was maintained at a steady power using only the shim rod, while moderator temperature varied steadily because of heat input from the circulating pump. Temperatures were recorded on the under-core resistance thermometer, mentioned in Section 5.1. The critical shim rod settings were then converted into reactivity changes, using the measured shim rod sensitivity data, and a least squares linear fit made to the reactivity-temperature data. This gave the result $\partial\rho/\partial T = -1.74 \times 10^{-5}$ $\delta k/k$ per degree F.

For the other assemblies, the collected data on critical shim rod settings and temperatures were examined, and comparable sets of readings used to calculate a temperature coefficient. These results were not very useful, ranging on each assembly from values of -10^{-4} up to $+5\times10^{-5}$. The lack of any consistent trend suggests that temperatures recorded were not representative of the core state at that time, whereas rod settings are immediately responsive to any change in conditions. For the critical mass extrapolation mentioned above, an absolute value of temperature coefficient is not in fact necessary.

6. DIFFERENTIAL NEUTRON SPECTRA

Methods of extracting a neutron beam from the assembly centre have been covered in Section 2 and 3 above. In addition, work done with the time-of-flight spectrometer has been fully reported by Tattersall (1967b). For completeness, equipment parameters and results are summarised here.

6.1 Spectrometer Parameters

All measurements on beams from assemblies 1 to 5 used a stainless steel chopper rotor. For assemblies 1, 2 and 3 a single speed of 1800 rev min^{-1} was used, while on assemblies 4 and 5 speeds of both 1800 and 7200 rev min^{-1} were used. The higher speed became possible through the use on assemblies 4 and 5 of a lithium glass scintillator detector, with usable efficiency at the higher neutron energies resolvable at this speed. Assemblies 1, 2 and 3 were examined with a bank of boron trifluoride proportional counters. The latter limited the useful energy range of the spectrometer to 0.01 to 10 eV, while with the lithium glass scintillator a range of 0.01 to 150 eV was possible.

Other aspects of the spectrometer arrangements depended on the type of detector used. Since the BF_3 counters were relatively insensitive to gamma rays, and had low efficiency for neutron detection, collimation and background shielding were designed with emphasis on reduction of neutron background. Zero flight time was obtained in this case from the gamma-ray response of a sodium-iodide scintillator placed behind the BF_3 counters. On the other hand, the lithium glass scintillator, as well as being very efficient for neutron detection, was sensitive to gamma rays. Thus collimation and background shielding for this detector were oriented towards gamma rays rather than neutrons. The gamma-ray response of the detector itself was used for setting zero flight time.

Flight path from assembly centre to chopper rotor was about 1.5 metres, while that from rotor to detector was about 7.5 metres. The beam path is shown in Figure 9.

Detector signals were received by a 512 channel time analyser with channel widths of 32 and 8 microseconds being used for speeds of 1800 and 7200 rev min^{-1} respectively.

6.2 Results

Each spectrometer run lasted for about three hours (three hours for each speed if two were used) at a source flux of about 10^9 n cm^{-2} sec^{-1} (Westcott subcadmium flux). Flux was restricted to this level to minimise a build-up of activity in the assembly fuel. Since the fuel loading for different assemblies could only be altered by hand, fission product radiation levels had to be kept low. A flux of 10^9 n cm^{-2} sec^{-1} was a compromise between activity build-up and attainable statistical accuracy in counting neutrons with the spectrometer.

The time analysis system used could have accepted a higher source flux level, since the combination of low source flux, chopper speed, and flight-path geometry led to a neutron reception rate at the detector of much less than one per burst; only about one neutron per four bursts was actually received.

To obtain uniform statistical accuracy, counts in analyser channels were grouped together. The criterion for grouping was to produce a 5 percent statistical accuracy where lithium glass was the detector, but the lower count rate from the BF_3 counters reduced the accuracy in that case to 15 percent.

Several corrections to the raw data were required before a spectrum could be produced. These corrections included:

(i) dead time (errors small)

(ii) background

(iii) air attenuation

(iv) slit transmission

(v) counter efficiency

(vi) air source.

These corrections are dealt with in full by Tattersall (1967a and b) and by Dalton (1969), and will not be further discussed here.

The corrected experimental spectra for assemblies 1 to 5 are shown in Figures 10 to 14 respectively. Also shown on these Figures are epithermal spectra measured with activation detectors (Section 7) and calculated spectra (Section 10). The experimental spectra clearly demonstrate the presence of a Maxwellian peak followed by an epithermal region which at least approximates to a 1/E law for the more dilute assemblies. As a higher proportion of fuel is added, the Maxwellian peak moves to higher energy and also becomes lower in magnitude relative to the epithermal component. The position of the peak on an energy scale moves from 0.061 eV (BeO : ^{235}U ratio of 6545 : 1) to 0.087 eV (ratio 740 : 1); thus even the most dilute assembly has a Maxwellian with the peak energy exceeding 0.025 eV the peak of the thermalised Maxwellian spectrum.

7. EPITHERMAL NEUTRON SPECTRA

Resolution of the time-of-flight spectrometer deteriorates in the epithermal region. Additional measurements of spectra in this region were made by a method utilising the activity of thick and thin resonance detectors and their measured cadmium ratio. Connolly et al. (1968) reported this work in more detail and pointed out that their method is independent of assumptions about spectrum shape and of indication of a spectrum parameter (for example, the Westcott method). Flux values at discrete energies are derived in the analysis, and the method gives epithermal differential spectra from irradiations of integral detectors.

The flux per unit energy ϕ_r at a resonance energy E_r is given (Connolly et al. 1968) by

$$\phi_r = \frac{(\sigma_{oD}/\sigma_{oA})\Delta_A \left[\alpha_D\{(G_D - T)/(1-T)\} - \alpha_D^*\{(G_D^* - T)/(1-T)\}\right]}{[\pi\Gamma\sigma_{r\gamma}/2]_D \left[f(\theta,\tau) - f^*(\theta,\tau^*)\right]_D}$$

where σ_{oD} = 2200 m/sec activation cross section of a detector

σ_{oA} = 2200 m/sec activation cross section of a gold detector

Δ_A = subcadmium saturation activity of a thin gold detector

α_D = $(R-1)^{-1}$ for a detector

G_D = subcadmium flux perturbation due to the detector

T = cadmium cover transmission correction

Γ = total width of the principal resonance of the detector

$\sigma_{r\gamma}$ = peak activation cross section of the principal resonance

$f(\theta, \tau)$ = resonance self-shielding factor

and the asterisks denote quantities relating to thick foils.

Accurate determination of the cadmium-ratio dependent quantity α is necessary, since the above equation shows that ϕ depends on the difference between α and α^*. It can be shown that the ratio $k = \alpha/\alpha^*$ is a true measure of epithermal reaction rate ratios for a thin and thick foil if $G = G^*$ If the latter is not the case, an apparent ratio k' is obtained, and we find

$$\frac{d\phi}{\phi} = -\left(\frac{k}{k-1}\right)\frac{dB}{B} = \left(\frac{k}{k-1}\right)\frac{dk'}{k'} \quad ,$$

where $B = \left(\frac{G_D - T}{1-T}\right)$

Values of k between 1.1 and 2.5 were obtained for the pairs of detectors used in this work; higher values of k usually involve self-shielding of more than one resonance.

Materials from which thin and thick foils were made were ^{103}Rh, ^{115}In, ^{197}Au, ^{186}W, ^{59}Co and ^{55}Mn. Each foil was ¼ inch in diameter, backed by a ½ inch diameter 0.001 inch thick, aluminium disc. Foils were irradiated either in aluminium boxes or cadmium boxes of wall thickness 0.015 inch. Foil thicknesses used, in terms of surface density, are shown in Table 11.

Both a detector foil and a monitor foil were irradiated together in a 1 inch diameter graphite 'rabbit' and analysed alternately with a 4π sodium iodide detector, thereby eliminating problems of amplifier gain drift, reactor power variation, and time measurement. Foils were located by BeO spacers in the rabbit (Figure 15) and inserted into the one-inch diameter tube arrangement (Section 2.1).

Flux values for assemblies 3, 4 and 5 are given in Table 12, and plotted in Figures 12, 13 and 14.

The results for epithermal fluxes in these assemblies are noteworthy initially in respect of the 1/E dependence visible for assembly 3, in which the BeO : ^{235}U ratio is 2250 : 1, but absent in assemblies 4 (1120 : 1) and 5 (740 : 1). It may be concluded that moderator to fuel ratios of the order of 2000 : 1 or greater are required in BeO : ^{235}U systems for 1/E dependence of the epithermal flux. This also implies that systems in excess of the 2000 : 1 ratio are sufficiently dilute for absorption in the epithermal region to be neglected compared with scattering, ($\Sigma_a << \Sigma_s$) in considering the slowing-down process.

8. FISSION RATE RATIOS

A third method of spectrum measurement was used on assemblies 2 to 5 inclusive, by recording count-rates of pulse ion chambers containing foils of various fissile materials. The gas-flow ion chambers used had parallel-plane geometry.

TABLE 11

CROSS SECTION DATA FOR FOIL DETECTORS

Isotope	Isotopic Abundance	σ_0 (barns)	E_r (eV)	Γ_n (meV)	Γ_γ (meV)	g	$\frac{\pi}{2}\Gamma\sigma_{r\gamma}$	Surface Density		G	G*	$f(\theta,\tau)$	$f^*(\theta,\tau^*)$	$\frac{\sigma_0}{\frac{\pi}{2}\sigma_{r\gamma}\Gamma[f(\theta,\tau)-f^*(\theta,\tau^*)]}$	Remarks
								Thin Foil $mg\ cm^{-2}$	Thick Foil $mg\ cm^{-2}$						
^{103}Rh	100%	149±4 both levels	1.257	0.78 ±0.01	155 ±4	0.5	1225 ±45	31.6	158.0	0.930	0.775	0.630	0.340	0.393 ± 0.21	Thermal yield ratio 0.075, resonance yield 0.080
^{115}In	95.72%	202±2 both levels	1.457	3.04 ±0.05	72±2	0.55	4524 ±77	1.81	5.7	1.0	0.970	0.820	0.640	0.249 ± 0.005	
^{197}Au	100%	98.8 ± 0.2	4.906	15.6 ± 0.4	124 ±3	0.625	7721 ±303	1.67	50.0	1.0	0.960	0.882	0.335	0.025 ± 0.001	
^{186}W	28.41%	37.8 ± 1.2	18.8	318	44	1.0	8390	49.0	171.5	1.0	0.980	0.705	0.467	0.0185	Errors discussed in text
^{59}Co	100%	37.4 ± 0.3	132.0	4.68 ±0.15 (eV)	0.67 ±0.15 (eV)	0.562	11145 ±2452	44.0	110.0	0.955	0.904	0.576	0.430	0.023 ± 0.005	Thermal and resonance yield ratios equal
^{55}Mn	100%	13.3 ± 0.2	335.5	22.35	0.45 ±0.04 (eV)	0.417	2241 ±268	13.2	87.0	0.995	0.965	0.941	0.760	0.028 ± 0.003[a]	1/E spectrum between 335.5 eV and 1098 eV
			1098	14.58 ± 0.7 (eV)	0.45 ±0.04 (eV)	0.583	963 ± 85					0.907	0.691		

(a) includes the contribution of the 1098 eV resonance

TABLE 12

EPITHERMAL FLUXES MEASURED IN ASSEMBLIES

	ACTIVATION DETECTOR					
	^{103}Rh	^{115}In	^{197}Au	^{186}W	^{59}Co	^{55}Mn
ASSEMBLY 3	U5:BeO = 1:2250		T = 0.058		$(\Delta/\sigma_o)_A$ = 1.70 x 10^9	
R	–	1.617 ± 0.005	1.485 ± 0.009	1.907 ± 0.007	5.64 ± 0.11	7.18 ± 0.03
R*	–	1.820 ± 0.004	2.20 ± 0.01	2.47 ± 0.01	6.77 ± 0.05	7.71 ± 0.1
$E_r \phi_r$ x 10^{-8}	–	2.84 ± 0.03	2.7 ± 0.1	2.73 ± 0.05	2.7 ± 0.3	3.0 ± 0.13
ASSEMBLY 4	U5:BeO = 1:1120		T = 0.087		$(\Delta/\sigma_o)_A$ = 1.29 x 10^9	
R	–	1.420 ± 0.005	1.330 ± 0.008	1.552 ± 0.006	3.54 ± 0.12	4.90 ± 0.02
R*	–	1 538 ± 0.003	1.735 ± 0.007	1.882 ± 0.008	4.05 ± 0.05	5.24 ± 0.02
$E_r \phi_r$ x 10^{-8}	–	2.87 ± 0.14	2.55 ± 0.1	3.30 ± 0.08	3.3 ± 0.8	3.6 ± 0.2
ASSEMBLY 5	U5:BeO = 1:740		T = 0.151		$(\Delta/\sigma_o)_A$ = 1.05 x 10^9	
R	–	1.288 ± 0.004	1.22 ± 0.02	1.350 ± 0.005	2.94 ± 0.06	3.29 ± 0.01
R*	–	1.367 ± 0.003	1.461 ± 0.004	1.536 ± 0.007	3.72 ± 0.03	3.714 ± 0.007
$E_r \phi_r$ x 10^{-8}	–	3.4 ± 0.2	2.8 ± 0.5	4.0 ± 0.1	5.4 ± 0.5	8.5 ± 0.2

8.1 Fission Chambers

The fission chamber design provides 2π collection geometry for fission-fragment-produced ionisation, and accurate location of the fissile coated foils.

The foils were one-inch diameter, 0.010 inch thick, platinum discs, on which deposits of the oxides of uranium, or of plutonium, were electroplated; the deposited material occupied an area with diameter of half-an-inch.

The compositions of the foils, as given in assays provided by the material supplier, are shown in Table 13. Foils were housed in an aluminium chamber assembly (Figure 16). The chamber body had two long aluminium tubes attached, forming inlet and outlet lines for the filling gas; a coaxial cable ran down the centre of one of the tubes, passing through an epoxy resin seal to the high-voltage electrode. The latter was an aluminium disc set parallel to the foil, and spaced a quarter inch from it; the foil formed the grounded electrode. Signal and high voltage connection was via a BNC connector mounted at the end of the gas lines.

To simplify filling a continuous flow of 90 percent argon/10 percent methane gas mixture was used; the outlet line was connected to a glycerine filled wash-bottle (to remove any foil material carried over by the gas), and the gas bottle reducer valve was adjusted to give a flow of about one bubble per second visible in the wash-bottle.

TABLE 13

FOIL COMPOSITIONS

Foil	^{232}U	^{233}U	^{234}U	^{235}U	^{236}U	^{238}U	^{239}Pu	^{240}Pu	^{241}Pu	^{242}Pu
^{233}U	10.8 p.p.m.	87.87%	0.83%	0.09%	0.03%	11.21%	–	–	–	–
^{235}U	–	–	0.57%	95.27%	–	4.16%	–	–	–	–
^{238}U	–	–	–	0.05%	–	99.95%	–	–	–	–
^{239}Pu	–	–	–	–	–	–	99.83%	0.17%	–	–
^{240}Pu	–	–	–	–	–	–	23.82%	74.01%	2.06%	0.11%

8.2 Mass Determination

In principle the fission chambers could have been used for absolute measurements, since they presented known good geometry. However determination of mass of the coatings was only possible for the ^{233}U foil; that of other foils had to be inferred indirectly. Actual weighing was not satisfactory, since various materials other than the fissile material were present in uncertain proportions.

The mass of the ^{233}U foil was determined by alpha counting in good 2π geometry conditions, using a solid state detector. Only small corrections were necessary for self-absorption and back-scattering for the thin (20 $\mu g\ cm^{-2}$) foil under these conditions.

Knowing the isotopic composition and the respective alpha-decay rates, the measured disintegration rate enabled the quantity of material present to be calculated. This calculation is summarised in Appendix 2.

A calibration of all chambers in a known thermal spectrum would enable masses of other foils to be inferred by using the measured ^{233}U foil value. It was found, however, that results in the form of count-rate ratios were adequate for comparison with theory, and no use was made of foil weights as such.

8.3 Theory of Measurement Technique

The following treatment was developed for the case where a series of fission chambers is used to record count rates in a known thermal spectrum and in the assembly spectrum. The proportion of thermally fissile and other nuclides present is shown in Table 13.

Let a foil of total mass M_j contain partial isotopic masses m_i. The effective fission cross section of nuclide i in the assembly spectrum ϕ is then $\hat{\sigma}_i$ and in a thermal spectrum ϕ_o is $\hat{\sigma}_{oi}$.

Then the fission reaction rate for a foil of mass M_j and containing nuclides i is given by

$$R_j = \sum_i r_i = N_o \left[\sum_i (m_i/A_i)\hat{\sigma}_i \right] \phi \qquad (1)$$

and

$$R_{oj} = \sum_i r_{oi} = N_o \left[\sum_i (m_i/A_i)\hat{\sigma}_{oi} \right] \phi_o \qquad (2)$$

where A_i is atomic mass of element i.

Determination of a reaction rate for a particular nuclide requires that sufficient equations (1) and (2) are available to allow other variables to be eliminated. The subscripts 3, 5, 8, 9, 0, 1 are used to indicate respectively ^{233}U, ^{235}U, ^{238}U, ^{239}Pu, ^{240}Pu and ^{241}Pu.

For a mass m_5 of ^{235}U

$$r_5 = N_o (m_5/A_5)\hat{\sigma}_5 \phi \qquad (3)$$

$$r_{o5} = N_o (m_5/A_5)\hat{\sigma}_{o5} \phi_o \qquad (4)$$

and then the ratios as follows can be used:

$$\frac{r_i}{r_5} = \frac{m_i/A_i}{m_5/A_5} \frac{\hat{\sigma}_i}{\hat{\sigma}_5} \qquad (5)$$

and

$$\frac{r_{oi}}{r_{o5}} = \frac{m_i/A_i}{m_5/A_5} \frac{\hat{\sigma}_{oi}}{\hat{\sigma}_{o5}} \quad . \qquad (6)$$

In a thermal spectrum, values of $\hat{\sigma}_{oi}/\hat{\sigma}_{o5}$ are known, and a measurement of r_{oi}/r_{o5} enables the ratio m_i/m_5 to be derived. Correspondingly, m_i/m_5 being known, in a specific spectrum r_i/r_5 is measured, and the ratio $\hat{\sigma}_i/\hat{\sigma}_5$ may be found.

Thus, if relative values suffice, the ratio $\hat{\sigma}_i/\hat{\sigma}_5$ can be found from measurements in the two spectra. If absolute values are needed, then the mass m_5 will have to be established from other types of measurement, as mentioned in section 8.2 for mass m_3.

8.4 Thermal Calibrations

A set of thermal calibrations was carried out in the HIFAR X–36 Low Flux Facility. The spectrum in the latter was not accurately known and thus a second calibration took place in MOATA using a graphite core with arrangements for central location of the chambers.

The Westcott parameters of the neutron energy spectrum at the core centre were well known, having been carefully measured by Connolly, Rose and Wall (1963) to be $r = 0.0389$ and $T = 45\,^{\circ}C$.

The ratios $\hat{\sigma}_{oi}/\hat{\sigma}_{o5}$ were derived using the GYMEA code, which weighted individual group cross sections with group fluxes based on a Westcott spectrum with $r = 0.0389$ and $T = 45\,^{\circ}C$.

$$\frac{\hat{\sigma}_{o3}}{\hat{\sigma}_{o5}} = 0.9835 \; ; \qquad \frac{\hat{\sigma}_{o9}}{\hat{\sigma}_{o5}} = 1.5648 \; ; \qquad \frac{\hat{\sigma}_{o1}}{\hat{\sigma}_{o5}} = 1.9963 \quad . \qquad (7)$$

The assay values of significance to thermal calibrations were taken from Table 13 and quantities to be used with equation (6) can then be summarised as in Table 14.

Foil mass ratios are obtained from the foil count rates and are given in Table 15.

TABLE 14

DETERMINATION OF MASS RATIOS FROM THERMAL NEUTRON CALIBRATION

Foil	Nuclide i	$\frac{A_5}{A_i}$	$\frac{\hat{\sigma}_{0i}}{\hat{\sigma}_{05}}$	$\frac{m_i}{M_{foil}}$	Partial mass ratio from r_{0i}/r_{05} m_i/m_5	$\left(\frac{m_i}{m_5}\right)\left(\frac{M^{235}U}{M_{foil}}\right)$
^{233}U	^{233}U	1.0086	0.9835	0.8787	$0.9938\ m_3/m_5 = 0.9166\ (M^{233}_U/M^{235}_U)$	0.9223
^{235}U	^{235}U	1.0000	1.0000	0.9527	1.0000	
^{238}U	^{235}U	1.0000	1.0000	0.0005	$0.000525\ (M^{238}_U/M^{235}_U)$	0.000525
^{239}Pu	^{239}Pu	0.9833	1.5648	0.9983	$1.5387\ m_0/m_5 = 1.6124\ (M^{239}_{Pu}/M^{235}_U)$	1.0479
^{240}Pu	^{239}Pu	0.9833	1.5648	0.2383	$1.5387\ m_9/m_5 = 0.3847\ (M^{240}_{Pu}/M^{235}_U)$	0.2500
	^{241}Pu	0.9751	1.9963	0.0206	$1.9466\ m_1/m_5 = 0.0420\ (M^{240}_{Pu}/M^{235}_U)$	0.0216
					$\sum_{i=9,1} r_{0i}/r_{05} = 0.4267\ (M^{240}_{Pu}/M^{235}_U)$	

where M^{233}_U, M^{235}_U, M^{238}_U, M^{239}_{Pu}, and M^{240}_{Pu} refer to the total masses of material on the (nominally) ^{233}U, ^{235}U, ^{238}U, ^{239}Pu and ^{240}Pu foils respectively.

TABLE 15

DETERMINATION OF FOIL MASS RATIOS

Chamber Foil	Foil Counting Rate (c.p.s.)	r_{0i}/r_{05}	$\frac{M_{foil}}{M^{235}U\ foil}$
^{233}U	2679.7 (1± 0.001)	1.518 (1± 0.002)	1.656 (1± 0.002)
^{235}U	1765.5 (1± 0.001)	1.000	1.000
^{238}U	7.26 (1± 0.005)	0.00411 (1± 0.006)	7.829 (1± 0.006)
^{239}Pu	2034.2 (1± 0.001)	1.152 (1± 0.002)	0.714 (1± 0.002)
^{240}Pu	1485.7 (1± 0.001)	0.842 (1± 0.002)	1.973 (1± 0.002)

8.5 Measurements on BeO-^{235}U Assemblies

The fission chambers were used on Assemblies 2 to 5 inclusive. In each case the aluminium experiment container holding the assembly was fitted with a two-inch internal diameter aluminium tube. The chambers were inserted one at a time into this tube through the beam port in the north cavity door, and reproducibly located in the centre of the experiment container by means of an aluminium locating jig. The south end of the tube was closed by graphite stringers filling the southern access hole through the graphite external reflector. Gas and electrical connections were made to each counter at the end of the filling tubes, which protruded from the north cavity door

During measurements, reactor power was held constant by manual adjustment of the regulating rod. An expanded-scale recorder was used as the power indicator. Signals to the recorder were derived from the servo-channel ion chamber, and amplified by a d.c. micromicroammeter. Reactor power was adjusted so that the current on this amplifier was set to 2×10^{-8} amps for all these measurements. A fixed backing-off potentiometer setting was used. Readings were only taken when the recorder showed reactor power to be constant, and all readings were normalised to correspond to recorder indication of 0.5 mV.

Conventional counting equipment was used (A.E.R.E. type 1430A head and main amplifiers). In some cases a Tennelec TC150 solid-state head amplifier modified for fission chambers was used but some amplifier oscillations were experienced with it. They were caused by poor earth continuity through epoxy resin joints on the gas tubes and chamber body and this fault, rather than the head amplifier itself, may have caused the earlier problems. Main amplifier output was always monitored by an oscilloscope, and pulse shaping set by amplifier integrating and differentiating time constants of 0.32 μsec.

For each fission chamber on each assembly, bias curves were taken and a suitable working point chosen before accumulating counts. In this case, counting was carried out as a function of time, with constant reactor power and hence neutron flux being maintained as described above.

The neutron flux at the chamber location was somewhat dependent on shim-safety rod position. As far as possible all measurements on any one assembly were carried out with shim rod position fixed.

Results are given in Table 16, and results as a ratio to the ^{235}U chamber are given in Table 17.

TABLE 16

ASSEMBLY COUNT RATES WITH FLUX LEVEL ERRORS INCLUDED
(Counts per second)

Chamber	Assembly			
	2	3	4	5
^{233}U	2169.7±1.0%	2056.1±1.0%	1845.9±1.0%	1448.6±1.0%
^{235}U	1371.9±1.0%	1251.7±1.0%	1038.8±1.0%	749.4±1.0%
^{238}U	5.87±1.3%	5.96±1.3%	4.55±1.5%	3.48±1.5%
^{239}Pu	1630.7±1.0%	1671.0±1.0%	1468.6±1.0%	1174.9±1.0%
^{240}Pu	–	1189.6±1.0%	–	869.1±1.0%

TABLE 17

INTEGRAL FISSION RATIOS RELATIVE TO ^{235}U IN BeO– ^{235}U ASSEMBLIES

Chamber	Assembly			
	2	3	4	5
^{233}U	1.582 ± 1.4%	1.643 ± 1.4%	1.777 ± 1.4%	1.933 ± 1.4%
^{235}U	1.0	1.0	1.0	1.0
^{238}U	0.00428 ± 1.6%	0.00476 ± 1.6%	0.00438 ± 1.8%	0.00464 ± 1.8%
^{239}Pu	1.189 ± 1.4%	1.335 ± 1.4%	1.414 ± 1.4%	1.568 ± 1.4%
	–	0.950 ± 1.4%	–	1.160 ± 1.4%

No dead-time corrections were made to the counting data. No significant dead-time effects were evident at count rates up to 5500 per second.

It was assumed that spectra in these assemblies were soft. Consequently, negligible fission rates were obtained in the non-thermally-fissile nuclides. Hence in analysing fission ratios in these assemblies, only the thermally-fissile constituents of the chamber foils were taken into account. A more elaborate analysis is possible in which all constituents are considered, but this was not done.

Thus the mass ratios (m_i/m_5) (M^{235}_U/M_{foil}) given in Table 14 and mass ratios (M_{foil}/M^{235}_U) given in Table 15 provide the following mass ratios for contained thermally-fissile nuclides:

TABLE 18

RELATIVE MASS RATIOS OF FOILS

Foil	Nuclide i	$\left(\frac{m_i}{m_5}\right)\left(\frac{M^{235}_U}{M_{foil}}\right)$	$\frac{M_{foil}}{M^{235}_U}$	$\frac{m_i}{m_5}$	$\left(\frac{m_i}{A_i}\right)\left(\frac{A_5}{m_5}\right)$
^{233}U	^{233}U	0.9223	1.656	1.527 (1±0.002)	1.540 (1±0.002)
^{238}U	^{235}U	0.000525	7.829	0.00411 (1±0.006)	0.00411 (1±0.056)
^{239}Pu	^{239}Pu	1.0479	0.714	0.748 (1±0.002)	0.736 (1±0.002)
^{240}Pu	^{239}Pu	0.2500	1.973	0.493 (1±0.002)	0.485 (1±0.002)
	^{241}Pu	0.0216	1.973	0.0426 (1±0.002)	0.415 (1±0.002)

Equation (5) and the values in Table 17 are now utilised to give the required quantities σ_i/σ_5 for each assembly.

TABLE 19

INTEGRAL FISSION CROSS SECTION RATIOS FOR INDIVIDUAL ASSEMBLIES

Assembly	Foil	Measured Ratio (r_i/r_5)	$(m_i/A_i)/(m_5/A_5)$	$\hat{\sigma}_i/\hat{\sigma}_5$
2	^{233}U	1.582(1±0.014)	1.540(1±0.002)	1.027(1±0.014)
	^{238}U	0.00428(1±0.016)	0.00411(1±0.006)	1.041(1±0.017)
	^{239}Pu	1.189(1±0.014)	0.736(1±0.002	1.615(1±0.014)
3	^{233}U	1.643(1±0.014)	1.540(1±0.002)	1.067(1±0.014)
	^{238}U	0.00476(1±0.016)	0.00411(1±0.006)	1.158(1±0.017)
	^{239}Pu	1.335(1±0.014)	0.736(1±0.002)	1.814(1±0.014)
	^{240}Pu	0.950(1±0.014)	0.485(1±0.002) (^{239}Pu content)	1.687(1±0.015) ($^{241}Pu/^{235}U$ ratio)
4	^{233}U	1.777(1±0.014)	1.540(1±0.002)	1.154(1±0.014)
	^{238}U	0.00438(1±0.018)	0.00411(1±0.006)	1.066(1±0.019)
	^{239}Pu	1.414(1±0.014)	0.736(1±0.002)	1.921(1±0.014)
5	^{233}U	1.933(1±0.014)	1.540 (1±0.002)	1.255 (1±0.014)
	^{238}U	0.00464(1±0.018)	0.00411 (1±0.006)	1.129 (1±0.019)
	^{239}Pu	1.568 (1±0.014)	0.736 (1±0.002)	2.130 (1±0.014)
	^{240}Pu	1.160 (1±0.014)	0.485 (1±0.002) (^{239}Pu content)	3.059 (1±0.015) ($^{241}Pu/^{235}U$ ratio)

Values for the ^{240}Pu chamber for Assemblies 3 and 5 have been treated as if the $\hat{\sigma}_9/\hat{\sigma}_5$ ratio were determined by the ^{239}Pu measurement. The result is then a value of $\hat{\sigma}_1/\hat{\sigma}_5$ as shown.

The result for the ^{238}U chamber is taken to be an indication that the nominal assay of 0.05 percent ^{235}U content is in error. No accuracy was quoted in the assay, and clearly a small percentage error in the assay could lead to a large change in ^{235}U content at the 0.05 percent level. In theory, for fission contributions due only to ^{235}U in the ^{238}U chamber, the ratio $\hat{\sigma}_i/\hat{\sigma}_5$ (which for this chamber is of course $\hat{\sigma}_5/\hat{\sigma}_5$) should be unity, allowing for experimental uncertainties.

Wherever possible, the precision of results and derived quantities has been expressed as a percentage of the number concerned. The error quoted refers to the standard deviation.

For count rates measured with the chambers, errors quoted include usual counting statistics: that is, $\sqrt{n}$, together with a 1 percent contribution due to reactor power level variations. No other error, such as location, was considered to make a significant contribution.

9. REACTIVITY MEASUREMENTS

Reactivity measurements were made with a series of materials on each of the five BeO-^{235}U assemblies. In each case, suitable quantities of the materials concerned were alternately placed in and removed from the assembly centre, and the resulting reactor periods measured. Two methods of recording reactor power data were used, in one case, direct on a recorder chart, and in the other, punched paper tape. This section gives details of equipment, methods and analysis technique employed for these measurements and quotes results for each assembly in terms of reactivity worth of materials.

9.1 Methods

Details of the materials used in reactivity measurements are given in Table 20. In some cases they were fitted into aluminium cans, while in others solid materials were used on their own. In all cases, the resulting sample was in the form of a right circular cylinder, of diameter approximately 0.475 inches. These cylinders were a sliding fit in the inner of two concentric tubes forming the pneumatic oscillator or transfer device. The oscillator, (Figure 17), had the two tubes arranged so that regulated high pressure air from the site air supply could be applied either to the central tube or to the annulus between the two tubes. This enabled the sample to be blown in either direction and thus positioned at either end of the inner tube.

The air supply to the oscillator was controlled by solenoid-operated valves; the latter received power from a control unit and power supply forming part of the Series 173 Digital Voltmeter Read Out equipment (Ellis 1967).

The oscillator itself was used by inserting it in the two inch diameter hole passing through each assembly, and by locating it so that the sample was close to the assembly centre on the 'IN' position (see Figure 1). The oscillator had to be removed from the reactor for sample changing.

The reactor power used for reactivity measurements was nominally 3 watts, corresponding to 2×10^{-8} amps on the installed linear power channel. With the oscillator loaded into the reactor, power was adjusted by appropriate movements of control rods such that the repetitive insertion and withdrawal of the sample caused the reactor power to fall and rise alternately, and the respective positive and negative periods were approximately equal.

All samples used gave small reactivity effects, corresponding to periods of hundreds or thousands of seconds. Samples were left in either the 'IN' or the 'OUT' position for times of the order of 400 seconds, which enabled linear rates of rise or fall of reactor power to be observed and recorded. Each set of measurements consisted of six complete cycles of the sample.

The reactor power behaviour during each measurement was recorded in two separate ways. In the first method, an in-core ion-chamber supplied current proportional to reactor power to a d.c. amplifier fitted with current suppression circuits. The mean current was backed-off as required, and the varying component, now appearing as the output voltage from the amplifier, fed to a digital voltmeter. The latter formed part of the Series 173 equipment, and was arranged so that it sampled the voltage at regular intervals, selectable to suit the data being acquired. In most cases, the sampling period was 2 seconds. When the sampling took place, the digital voltmeter reading, together with information on sample location, was punched out on paper tape. Thus the numbers coded on the tape represented the complete power history of the reactor on a scale expanded in accordance with the degree of current suppression used at the d.c. amplifier.

The control unit of the Series 173 equipment actuated the oscillator air solenoids, providing a square wave switching pattern of selectable period for use in an automatic sample moving sequence. The period most commonly used in these measurements was 800 seconds, allowing the sample to remain 'IN' or 'OUT' for 400 seconds each. Manual control was also provided to enable the sample to be moved at will. Figure 18 shows a schematic diagram of this part of the equipment.

The second method of recording reactor power used a switched-range chart recorder, with built-in back-off facilities. The input to the recorder came from the voltage output of the installed linear channel d.c. amplifier. A separate ion-chamber supplied this channel. Figure 19 shows a schematic diagram of this equipment.

TABLE 20

DETAILS OF MATERIALS

Sample No.	Material	Physical Form	Mass (grams)	Other Contents	Can	Mass of Can (grams)
3	^{235}U	0.002 inch foil	0.09539	–	Al	3.26
5	BeO	Solid sintered	3.9336	–	Al	2.32
6	Steel	Solid	18.6	–	–	–
7	Polythene	Solid	0.7898	–	–	–
8	Polythene	Solid	2.1742	–	–	–
9	Graphite	Solid	3.8828	–	–	–
10	Graphite	Solid	3.8636	–	–	–
11	Aluminium	Solid	6.6611	–	–	–
12	Boron carbide	Powder	0.05115	Al powder	Al	3.91 powder + can
13	Natural uranium	Solid	30.0	–	Al	1.9
14	Aluminium	Solid	12.8767	–	–	–
15	Graphite	Solid	4.1925	–	–	–
17	Natural uranium	Solid	30.0	–	Al	1.11
19	^{235}U	0.002 inch foil	0.6438	–	Al	1.59
22	Molybdenum	Solid	11.438	–	Al	1.65
23	Nickel	Solid	21.11	–	–	–
25	Polythene	Solid	2.1742	–	–	–
27	^{235}U	0.002 inch foil	0.0825	–	C	4.32
29	Natural uranium	Solid	31.11	–	Al	0.59
31	Gadolinium	0.0001 inch foil	0.515 mg	–	Al	2.02
33	Cadmium	0.026 inch foil	0.0497	–	Al	6.39
34	Chromium	Flake	5.076	–	Al	1.60
35	Boron-10	Powder	1.662 mg	Al powder	Al	4.870 powder + can
36	Boron-10	Powder	3.149 mg	Al powder	Al	4.916 powder + can
37	^{233}U-Oxide	Powder	100.7 mg	Al powder	Al	1.691 powder + can
41	Iron	Solid	5.84	–	Al	2.22
44	Boron-10	Powder	0.6714 mg	Al powder	Al	4.87 powder + can
46	Graphite	Solid	7.8486	–	–	–
47	BeO	Solid (sintered)	4.7988	–	Al	2.21

Although both recording methods are basically similar, in backing-off and then scaling-up an ion-chamber signal, the purpose of using both was to provide an immediately visible and approximately analysable record (the chart records) together with a record which could be processed by computer at a later stage (the punched paper tape).

9.2 Analysis

Samples used, and their reactivities, were of such a magnitude that in most cases the asymptotic period obtained enabled the reactor power to be closely approximated by a linear function of time. This approximation was used explicitly in the case of chart records, where a straight line was manually fitted to the power trace, and the slope of the line was used in determining the period. Reduction of data recorded on paper tape did not use this linear approximation, as a logarithmic fit was made to the power records.

When fitting the chart records, initial transients and evident non-linearities were omitted. The fitted straight line having been found, data were recorded on punched cards to enable the slope to be calculated by computer. Appendix 3 describes the calculation of the parameters used and refers to the simple computer programme RCA. Computer calculation avoided arithmetic errors in large numbers of repetitive manual calculations, and gave ready printed tables in a standard format.

The format and significance of numbers recorded on punched paper tape in this work, as well as details of editing, collating, and listing programmes, are given in Appendix 4. In this case, after correction and listing of the data and storage on magnetic tape, a programme RAC was used to select and analyse data for particular sets of reactivity measurements (see Appendix 5).

As mentioned in Section 9.1, the reactor was brought to a stable condition before commencing measurements. Small drifts in power, possibly due to temperature changes, occurred on some occasions. If they were not too severe, measurements were continued, but if substantial, the measurements were stopped until stability was restored. In the analysis, it is assumed that the reactivity worth of a given sample is the difference between the algebraic values of the reactivities derived from the 'IN' legs and from the 'OUT' legs. Thus the mean reactivity from a series of 'IN' legs, $\bar{\rho}_{IN}$, and the mean reactivity from a series of 'OUT' legs, $\bar{\rho}_{OUT}$, are combined to give the mean reactivity worth of the sample by the expression

$$\bar{\rho} = \bar{\rho}_{IN} - \bar{\rho}_{OUT} .$$

Moderate drifts in reactor power during several cycles do not affect this method of obtaining the sample reactivity, provided that the drifts are linear with time and that no other change is made to the reactor, such as movement of a control absorber. Both methods of analysis depend on this assumption.

The calculation of reactivity from period data was based on the inhour equation for an asymptotic period

$$\rho = (\ell/Tk_{eff}) + \sum_{i=1}^{6} [\beta_i/(1 + \lambda_i T)] ,$$

where the symbols have their usual meaning. The assumption was made that the first term on the right-hand side may be neglected, which for the periods used in these measurements involved an error of less than 1 percent.

Data for ^{235}U thermal fission (Keepin 1965) as shown in the following table were used:

Delayed Neutron Group	Relative Abundance $a_i = \beta_i / \beta$	Decay Constant (secs^{-1})
1	0.033	0.0124
2	0.219	0.0305
3	0.196	0.111
4	0.395	0.301
5	0.115	1.14
6	0.042	3.01

The value of β (also from Keepin) was taken as 0.00650.

9.3 Results

The series of measurements was exploratory and intended for evaluation of experimental techniques and the results must be viewed in that light. For instance, it was possible from computer fitting to paper tape data to obtain quantitative information on goodness-of-fit; hence confidence in the precision of the analysis was gained. On the other hand, manual fitting to chart records could apparently be somewhat inaccurate unless particular care was taken. Having conducted both types of analysis, it may be seen that in many cases remarkably good agreement was obtained between the manual and computer results; this was significant in that the manual results could be treated as reliable in regard to accuracy of fitting, while conversely there were no great problems in the handling of large masses of data through the computer.

In those cases where unresolved discrepancies existed between manual and computer results, it was highly likely that errors in recording of equipment parameters were the cause, making accurate analysis impossible. This problem highlighted the need for the closest personal scrutiny of the progress of measurements of this type, where accumulation of large quantities of data could be rendered useless by failure to record accurately some important control or equipment parameter. In this respect there was a very strong case for reducing manual recording to a minimum.

Results are presented first as actual reactivity values produced by the two analysis methods for each of the five assemblies, together with any relevant comments (Tables 21 to 25). Table 26 then lists the values selected for final analysis, and Table 27 quotes reactivity values per gram for each material studied.

TABLE 21

ASSEMBLY 1* REACTIVITIES DERIVED FROM ANALYSIS OF CHART RECORDS

Sample No.	Run No.	No. of Legs	Mean Values of Reactivity (10^{-6} δk/k)		
			$\bar{\rho}_{IN}$	$\bar{\rho}_{OUT}$	$\bar{\rho}$
13	1/2	9	-3.28	6.80	-10.1
11	1/3	8	-1.08	3.09	- 4.17
6	1/4	19	-16.6	8.0	-24.5
8	1/5	7	8.9	-13.2	22.2

* No paper tape records were made for this assembly

TABLE 22

ASSEMBLY 2 REACTIVITIES DERIVED FROM ANALYSIS OF CHART AND TAPE RECORDS

Sample No.	Run No.	Tape Records				Chart Records				Comments
		No. of Legs	Mean Values of Reactivity (10^{-6} δk/k)			No. of Legs	Mean Values of Reactivity (10^{-6} δk/k)			
			$\bar{\rho}_{IN}$	$\bar{\rho}_{OUT}$	$\bar{\rho}$		$\bar{\rho}_{IN}$	$\bar{\rho}_{OUT}$	$\bar{\rho}$	
13	01	4	−1.44	1.44	−2.87	12	1.37	−1.49	2.85	Opposite signs not explained; tape record data uncertain
3	03	8	7.70	−3.98	11.7	12	7.86	−4.08	11.9	
3	04	2	9.92	−3.97	13.9	Part of Run 03				
5	05	12	4.32	−2.82	7.14	13	4.26	−2.88	7.14	
12	17	8	−40.5	46.7	−87.2	13	−36.8	47.0	−83.9	
12	20	9	−44.6	45.4	−90.1	7	−39.4	43.9	−83.3	
10	21	13	4.54	−3.64	8.18	14	4.16	−3.35	7.51	
7	32	15	5.92	−3.90	9.82	14	5.61	−3.65	9.25	
6	41	10	−16.8	11.7	−33.9	12	−17.2	17.5	−34.8	
11	42	6	−2.37	0.97	− 3.34	11	− 2.59	0.93	− 3.51	
		4	−2.73	0.82	− 3.54	Tape restart				
11	43	6	−2.44	1.48	− 3.92	18	− 2.30	1.34	− 3.64	
		6	−2.60	1.18	− 3.79	Tape restart				

TABLE 23

ASSEMBLY 3 (SECOND RUN) REACTIVITIES DERIVED FROM ANALYSIS OF CHART AND TAPE RECORDS

Sample No.	Run No.	Tape Records				Chart Records				Comments
		No. of Legs	Mean Values of Reactivity (10^{-6} δk/k)			No. of Legs	Mean Values of Reactivity (10^{-6} δk/k)			
			$\bar{\rho}_{IN}$	$\bar{\rho}_{OUT}$	$\bar{\rho}$		$\bar{\rho}_{IN}$	$\bar{\rho}_{OUT}$	$\bar{\rho}$	
36	51	10	−35.3	29.6	−64.8	13	−26.1	23.9	−50.0	Poor fit for tape. Use chart
22	52	10	−18.0	16.8	−34.8	12	−13.9	14.0	−27.9	" " " "
12	53	12	−60.5	49.9	−110.4	11	−54.2	48.0	−102.2	
19	54	12	23.7	−28.0	51.7	13	19.9	−21.1	35.2	
35	55	10	−16.8	18.0	−34.8	19	−15.2	17.0	−32.2	
14	56	Invalid results								
						14	− 3.73	4.25	− 7.98	Tape questionable. Use chart
14	57	7	− 5.17	5.53	−10.70					
41	58	11	−11.8	13.7	−25.5	13	− 9.17	11.18	−20.4	
29	59	10	−15.2	11.0	−26.2	12	−11.88	9.27	−21.1	
37	60	4	3.87	−3.74	7.61	15	3.69	−3.78	7.42	
46	62		−0.170	−0.119	1.02	12	0.245	−1.007	1.25	Reactor drifting
27	63		3.03	−5.37	8.40	14	2.77	−4.24	7.01	" "
44	64	12	−8.09	10.75	−18.84	12	−6.50	9.15	−15.7	
31	65	Invalid results				3	−2.24	1.06	− 3.30	" "
31	66	10	−1.35	2.38	−3.72	11	−1.05	2.14	− 3.19	
33	67	10	−9.39	10.93	−20.3	12	−7.93	9.07	−17.0	
25	68	10	4.59	−4.19	8.78	12	3.78	−3.71	7.49	
5	69	12	−0.531	0.692	−1.22	12	−0.530	0.650	−1.18	" "
23	70	10	−55.9	49.3	−105.2	14	−44.2	45.0	−89.2	
34	71	12	−12.5	14.5	−27.1	13	−9.81	12.35	−22.2	
5/47	72	4	− 2.32	1.00	− 3.32	5	−1.41	1.00	− 2.41	" "
5/47	73	5	− 2.34	1.01	− 3.35	5	−1.84	0.92	− 2.76	" "
5/47	74	6	− 1.61	1.84	− 3.45	6	−1.25	0.93	− 2.18	

TABLE 24

ASSEMBLY 4 REACTIVITIES DERIVED FROM ANALYSIS OF CHART AND TAPE RECORDS

Sample No.	Run No	Tape Records				Chart Records				Comments
		No. of Legs	Mean Values of Reactivity (10^{-6} δk/k)			No. of Legs	Mean Values of Reactivity (10^{-6} δk/k)			
			$\bar{\rho}_{IN}$	$\bar{\rho}_{OUT}$	$\bar{\rho}$		$\bar{\rho}_{IN}$	$\bar{\rho}_{OUT}$	$\bar{\rho}$	
12	04	Not on tape				4	−40.5	51.7	−92.2	
12	05	Not on tape				12	−43.0	48.4	−91.4	
13	17	Not on tape				2	−8.0	8.36	−16.4	Insufficient data
14	18	Not on tape				16	11.1	−10.3	21.4	
9	21	Not on tape				17	14.1	−13.9	28.0	
7	22	Not on tape				3	22.3	−17.1	39.4	
7	23	Not on tape				10	22.5	−16.2	38.7	
5	32	12	14.9	−16.6	31.4	13	14.2	−14.8	29.0	
3	34	4	18.6	−14.8	33.4	4	18.1	−13.4	31.5	
3	35	2	7.3	−25.0	32.3	2	7.0	−23.0	30.0	
3	36	4	12.4	−24.2	36.6	8	12.8	−18.5	31.3	
3	39	12	14.4	−15.8	30.2	12	15.7	−15.9	31.5	
6	41	10	−14.5	10.8	−23.2	12	−15.1	11.8	−26.9	
6	42	6	−15.6	10.7	−26.3	6	−15.8	11.3	−27.1	
14	58	Not on tape				7	11.4	−14.0	25.5	
12	59	6	−59.5	50.6	−110.0	6	−56.6	59.4	−116.0	
12	60	6	−57.4	52.1	−109.0	6	−53.7	60.6	−114.0	
13	61	6	−22.1	17.0	− 39.1	6	−20.6	19.7	− 40.3	
13	62	4	−16.8	18.9	− 35.6	2	−18.6	20.0	−38.7	
7	66	14	4.89	−4.92	9.81	14	5.27	−5.39	10.7	
14	67	2	−3.42	4.40	−7.83	2	−3.00	4.28	− 7.28	
14	68	12	−4.49	3.88	−8.37	12	−4.12	3.61	− 7.73	
17	69	4	−22.5	16.0	−38.4	4	−24.5	16.5	−40.9	
17	70	8	−21.4	18.5	−39.9	8	−19.4	18.3	−37.7	

TABLE 25

ASSEMBLY 5 REACTIVITIES DERIVED FROM ANALYSIS OF CHART AND TAPE RECORDS

Sample No.	Run No.	Tape Records				Chart Records				Comments
		No. of Legs	Mean Values of Reactivity (10^{-6} δk/k)			No. of Legs	Mean Values of Reactivity (10^{-6} δk/k)			
			$\bar{\rho}_{IN}$	$\bar{\rho}_{OUT}$	$\bar{\rho}$		$\bar{\rho}_{IN}$	$\bar{\rho}_{OUT}$	$\bar{\rho}$	
14	01	5	–1.89	4.56	–6.45	5	–1.89	4.40	–6.29	
14	02	6	–2.12	4.74	–6.86	6	–2.39	4.65	–7.04	
14	03	5	–3.60	3.22	–6.82	4	–3.43	3.15	–6.58	
7	04	12	12.2	–7.0	19.3	12	12.4	–6.6	19.0	
15	05	7	0.816	–0.311	1.13	7	2.04	–0.58	2.62	Poor fit to tape data. Tape record unreliable
15	06	2	0.71	–2.51	3.22	6	0.88	–2.32	3.20	
15	07	3	1.03	–2.28	3.30	Part of Run 06				
12	08	12	–46.0	58.1	–104.0	12	–38.6	67.9	–107.0	
5	09	6	1.43	–2.86	4.29	6	1.48	–2.79	4.27	
5	10	6	1.36	–1.47	2.83	6	1.90	–2.06	3.96	Suppression data for tape unreliable
6	12	12	–29.6	15.3	–44.9	14	–29.5	16.8	–46.3	
17	13	12	–24.4	22.2	–46.5	12	–25.3	26.3	–51.6	
19	27	11	4.24	–5.22	9.46	19	6.91	–8.03	14.9	Suppression data for tape unreliable

TABLE 26a

REACTIVITY VALUES SELECTED FOR FINAL RESULTS

(Reactivities in 10^{-6} $\delta k/k$)

Assembly		Materials							
		^{235}U	Natural U	BeO	Graphite	Polythene	Aluminium	Steel	Boron Carbide
1	Experimental result Sample No. Run Nos.	–	–10.1 13 1/2	–	–	22.2 8 1/5	–4.17 11 1/3	–24.5 6 1/4	–
2	Experimental result Sample No. Run Nos.	11.7 3 03	– 2.87 23 01	7.14 5 05	8.18 10 21	9.82 7 32	–3.65 11 42/43	–33.9 6 41	–88.7 12 17/20
3 (Second Run)	Experimental result Sample No. Run Nos.	52.7 19 54	–25.8 29 59	0.22 5 69	1.02 46 62	8.78 25 68	–7.98 14 56/57	24.7 41 58	–108.1 12 53
4	Experimental result Sample No. Run Nos.	33.1 3 34/35/36/39	–39.2 17 69/70	31.4 5 32	28.0 9 21	9.81 7 66	–8.10 14 67/68	–24.8 6 41/42	–110.0 12 59/60
5	Experimental result Sample No. Run Nos.	14.9 19 27	–46.5 17 13	4.29 5 09	3.26 15 06/07	19.3 7 04	–6.71 14 01/02/03	–44.9 6 12	–104.0 12 08

TABLE 26b

ADDITIONAL VALUES OBTAINED ONLY ON SECOND RUN OF ASSEMBLY 3

Assembly		Materials										
		B–10	B–10	B–10	Mo	^{233}U	^{235}U	Gd	Cd	Ni	Cr	BeO
3	Experimental result Sample No. Run Nos.	–46.9 36 51	–31.8 35 55	–14.8 44 64	–26.9 22 52	9.02 37 60	7.83 27 63	–2.47 31 66	–16.4 33 67	–105.2 23 70	–26.1 34 71	0.33 5/47 73/74

TABLE 27

REACTIVITY WORTHS PER GRAM OF MATERIAL

(Reactivities in 10^{-6} $\delta k/k$)

Assembly	Materials								
	^{235}U	Natural–U	BeO	Graphite	Polythene	Aluminium	Steel	Boron Carbide	^{238}U
1	–	–0.297	–	–	10.2	–0.626	–1.32	–	–
2	153.0	–0.061	2.14	2.12	12.4	–0.548	–1.82	–1690	–1.14
3 (2nd run)	88.1	–0.83	0.179	0.159	4.0	–0.620	–4.13	–2120	–1.46
4	398.0	–1.28	8.36	7.21	12.4	–0.629	–1.33	–2110	–4.10
5	28.9	–1.53	1.40	0.778	24.4	0.521	–2.41	–1990	–1.74

Notes: (1) Values quoted for ^{235}U, Natural–U, BeO and Boron carbide have been corrected for aluminium content of can.

(2) Values quoted for ^{235}U have been corrected for ^{238}U content, while those quoted for ^{238}U have been derived from Natural–U values, corrected for ^{235}U content, using the following expressions:

^{235}U (pure) = 1.0790 M1 – 0.0625 M2

^{238}U (pure) = –0.00761 M1 + 1.00749 M2

where M1, M2 are the measured values for ^{235}U and Natural–U respectively.

ADDITIONAL VALUES OBTAINED ONLY ON SECOND RUN OF ASSEMBLY 3

Assembly	B–10 (extrapolation to zero mass)	Mo	^{233}U	^{235}U	Gd	Cd	Ni	Cr	BeO
3	–24400	–2.35	104.8	94.9	–4804	–329	–4.98	–5.14	0.038

Three criteria were used to select values given in Table 27. First a check was made for consistency between separate sets of data on the same sample on the one assembly. Where inconsistency was evident, the only alternative course available was an arbitrary subjective judgement. Second, if there was reasonable correspondence between chart and tape data for the same run, the tape data was used on grounds of greater precision of analysis. Third, where tape data were unreliable or open to criticism on various grounds, chart values were used. The need and reasons for this selection technique are discussed above.

9.4 Comments

This series of measurements established a technique for finding reactivity values of small samples of materials. There were certain unsatisfactory aspects of the results presented, in that there remained some unexplained inconsistencies, and some gaps in the recording of accurate parametric and instrumental data. In addition there was a lack of systematic repetition of measurements to establish repeatability and it would have been valuable to have checked the linearity of results against several sizes of similar samples. These omissions arose partly from the shortage of available time and the intention primarily to evaluate the technique.

Comparing data collection by chart and tape, this part of the work made clear the vital importance of recording correct instrument settings for the tape data, since there were more opportunities for error here than for chart recording.

The principal advantages of the tape method included the absence of the need for any (subjective) manual estimation in curve-fitting, and the availability of quantitative error estimates. It was also an asset to be able to use alternative data analysis methods without further manual work.

10. THEORETICAL CALCULATIONS

10.1 General

When performing a series of calculations for which the measurements described above are intended as experimental checks, considerable geometrical difficulties appear. The under-moderation and heterogeneity of most of the assemblies requires a multi-energy group transport theory treatment. Thus multigroup transport codes were used in part and two-dimensional diffusion theory calculations were performed on a homogenised version of the assembly. An outline of the three-dimensional arrangement of assembly and reactor which had to be represented in two dimensions for calculational purposes is shown in Figure 20a.

Several attempts were made to find a credible two-dimensional representation. Spinks (1967) used the cylindrical r-z model of Figure 20b for diffusion theory calculations, together with transport-theory-derived diffusion parameters for the central homogenised assembly Tattersall (1967b) also used Spinks' model in calculating assembly spectra for comparison with chopper results.

Dalton (1969) developed and extended Tattersall's original work both in analysis of chopper data and in using a different geometrical model. Dalton's emphasis was in calculating spectra at the centre of assemblies for comparison with the measured spectra, and it was found that close agreement could in fact be obtained between theory and measurement. Curves showing the agreement reached are reproduced in Figures 10 to 14. It was concluded that the approximations made in the calculations were justified for the particular situation

If calculations such as Dalton's are to be applied or extended to permit comparison with other measurements, such as fission ratios or reactivity measurements, a further complication is apparent; the presence of the two-inch diameter hole through the assembly introduces another heterogeneity with an additional leakage path through the central region

The choice of data for the calculations is important. Cripps (1969) also performed calculations related to these assemblies using a locally modified version of the Los Alamos 18-group data set (Connolly 1963). Although this set does not contain cross sections for all materials of interest, the argument has been advanced that it has the advantage of having been checked against experiments. The need to modify the cross sections, particularly in the more thermal groups, to suit the type of spectrum involved in the present work, seems in one respect at least to nullify

the 'tested' aspect of the set. A further disadvantage appears to be the lack of any positive contribution to local endeavours to build up a combined data and multigroup calculational scheme such as GYMEA (Pollard and Robinson 1966). The latter, as part of an overall programme of theory plus experiment, needs to be tested and if shown lacking, to be modified to improve its utility. Ad hoc modifications to the Los Alamos set can have only a limited usefulness, and can hardly be referred back to basic data or calculational methods and approximations.

Thus data derived from GYMEA have in fact been used by Tattersall (1967b) and Dalton (1969) and by the author in the calculations described below.

10.2 Calculation of Spectra

As mentioned above, differential spectra were calculated by Dalton (1969) for comparison with chopper measurements. An initial attempt was made using Dalton's spectra to derive the fission rate ratios against the measured values described in Section 8. Thus the reaction rates for infinitely dilute fissile isotopes were calculated using 120 group fluxes as input to GYMEA. The thin foils used for the fission ratio measurements did not require any significant self-shielding correction.

This initial calculation showed that the central spectrum appropriate to the chopper measurements was less thermal than that existing when fission chambers were introduced. This conclusion was based on the fact that the measured ratios were smaller than the calculated ones, and that the ratios tended to decrease with increasing thermal content. These results applied to all assemblies.

The presence of a two-inch diameter hole through the assembly centre suggests that there would be an increase in epithermal leakage due to streaming down the tube, and hence a softening of the spectrum. In addition, the geometry of some assemblies required removal of fuel to make way for the tube. The reduction in fuel in the central region then led to decreased thermal absorption and a resulting enhancement of the spectrum in the thermal region. The overall result, it is suggested, was a softer spectrum when the tube was in place.

A series of calculations (which made allowance for the tube's presence) was then undertaken. The technique adopted was to simulate an assembly by three concentric circular regions. From the centre outward these were the central, standard cell and outer regions. The standard cell region was given a composition typical of that portion of the assembly where the nominal BeO/^{235}U ratio was unaffected by reflector material or the central tube arrangements. Composition of the outer region was similar to that of the standard cell region, except that allowance was made for additional BeO at top and bottom surfaces of the experiment container. The central region took account of the region immediately surrounding the tube, and thus had a more dilute composition than the other regions.

The composition of each region was used in a GYMEA-WDSN-GYMEA calculation (Doherty 1968) to produce cross sectional data for a homogenised version of each. Flux disadvantage factors were calculated within this scheme in the WDSN step (Francescon 1963). The cross sectional data were then used in an 18-group CRAM calculation (Hassitt 1962) which derived energy-dependent leakage values for the central point of a one-dimensional cylindrical model. Each region was represented as a circle (or annulus, as appropriate) together with an outer graphite ring as reflector. An axial buckling was included in the input data to allow for the finite length of the assembly and reactor.

The central mesh point leakage values were then supplied to a further 120-group GYMEA calculation for the central region, the output being a 120-group spectrum at the central point. Fission ratios were then calculated using this spectrum.

The major difficulty in applying this calculational scheme was found to be the choice of radii of the three fuelled regions, particularly the radius of the central region. A somewhat arbitrary selection had to be made of the boundary of the corresponding region of the assembly. In practice, the method of selection was based on fission ratios obtained from the infinite medium GYMEA-WDSN-GYMEA calculation for the central region. These ratios were an indication of spectrum hardness, and were made harder on applying the CRAM-derived leakages. Comparison with the measured values thus made possible an empirical adjustment to the region boundaries until reasonable agreement could be obtained between measurement and calculation.

10.3 Fission Ratios

The procedure described in Section 10.2 led to calculated values for the fission ratios σ_i/σ_5. Table 19 gave the measured values for these for Assemblies 2 to 5, and Table 28 summarises the comparison between experiment and theory.

TABLE 28

COMPARISON OF MEASURED AND CALCULATED FISSION RATIOS

Assembly Ratio $\hat{\sigma}_i/\hat{\sigma}_5$	2		3		4		5	
	Meas.	Calc.	Meas.	Calc.	Meas.	Calc.	Meas.	Calc.
$^{233}U/^{235}U$	1.03	1.05	1.07	1.09	1.15	1.14	1.26	1.27
$^{239}Pu/^{235}U$	1.62	1.72	1.81	1.83	1.92	1.94	2.13	2.19

The standard deviations of errors on the measurements are about 1.5 percent in all cases.

Examination of the $^{233}U/^{235}U$ and $^{239}Pu/^{235}U$ effective cross section ratios shows that the calculated values are within three standard deviations of the measured values in most cases. Both measured and calculated values change in the expected manner with decreased dilution of the assembly composition.

The question then arises as to the significance of the agreement between experiment and theory in this case. The sole way to answer this question is to point out that the measurements can only be described accurately by a three-dimensional model in x,y,z geometry. To perform any calculations at all, it is necessary to adopt one- or two-dimensional models. This immediately demands a number of arbitrary choices in setting up the representation of the physical system and there is no clear justification for one arbitrary choice against another.

Nevertheless the arbitrary choices made in selecting boundaries for the central and standard cell regions were consistent over the four assemblies for which the above results are presented. That is, similar boundaries were used in determining the material ratios in the central region for each assembly, and the same central region diameter was employed in each CRAM calculation. At worst, then, it could be argued that an empirical agreement was obtained on one assembly, and that parameters used for the empirical fit were found to give agreement for the remaining assemblies.

Only ^{233}U, ^{235}U and ^{239}Pu values have been regarded as significant in the above discussion, despite the inclusion of ^{238}U and ^{240}Pu results in Table 19.

In the latter two cases there was insufficient confidence in their isotopic composition, and the experimental fission ratios are considered to have little value.

10.4 Reactivity Values

If a material is introduced to or removed from a region of a reactor with flux ϕ, then the reactivity change is subject to the approximation of first order perturbation theory given by

$$\Delta\rho = \frac{\int_{\text{material}} \phi \Delta\sigma \phi^* \, dV}{\int_{\text{reactor}} \phi\psi\nu\Sigma_f\phi^* \, dV} ,$$

where $\Delta\sigma$ is the change in effective cross section σ consequent on the material introduction or removal, ϕ and ϕ^* are the flux and adjoint respectively, dV is an element of volume, and ψ, ν and Σ_f are the fission spectrum, neutron emission per fission and macroscopic fission cross section respectively.

To calculate $\Delta\rho$ in a given situation, it is necessary to know the effective cross sections for fission, absorption, scattering, etc. for the material concerned, together with the spectrum ϕ and its adjoint ϕ^* in the region of the reactor where the change takes place. If it is considered adequate to calculate only relative values of $\Delta\rho$, then the denominator (which remains constant for a given overall reactor situation) may be ignored.

In the present case, values of group fluxes ϕ_i and adjoint ϕ_i^* were obtained from the 18-group CRAM calculations referred to in Section 10.2. Fluxes at the central mesh point were printed out on cards using an option built into the CRAM code (McGregor et al. 1968).

A facility was incorporated in GYMEA (Pollard, private communication) to carry out the multiplications $\phi\Delta\sigma\phi^*$ and to integrate over the various cross sections and the group structure. This routine, known as CREAP (Central Reactivity Perturbation), also made provision for resonance self-screening in materials such as ^{238}U by calculating an appropriate mean chord length for the sample and carrying out a WDSN transport theory calculation to obtain disadvantage factors.

TABLE 29

COMPARISON OF MEASURED AND CALCULATED REACTIVITIES

Assembly	2		3		4		5	
	Meas.	Calc.	Meas.	Calc.	Meas.	Calc.	Meas.	Calc.
Natural U	–0.061	0.33	–0.83	–0.35	–1.3	–4.9	–1.5	–1.1
^{233}U	–	–	–	–	–	–	–	–
^{235}U	153	153	88	88	398	398	29	29
^{238}U	–1.1	–0.79	–1.5	–1.0	–4.1	–7.8	–1.7	–1.3
C	2.1	0.13	0.16	0.21	7.2	1.8	0.78	0.44
BeO	2.1	0.16	0.18	0.25	8.4	2.1	1.4	0.54
Al	–0.55	–0.41	–0.62	–0.45	–0.63	–3.1	–0.52	–0.39
^{10}B	–	–	–24400	–20000	–	–	–	–
^{56}Fe	–1.8	–2.3	–4.1	–2.6	–1.3	–18	–2.4	–2.4
Mo	–	–	–2.4	–1.5	–	–	–	–
Ni	–	–	–5.0	–4.2	–	–	–	–
Cr	–	–	–5.1	–3.2	–	–	–	–

Table 29 shows both measured and calculated values. The measured values, which have been abstracted from Table 27, are expressed in terms of 10^{-6} $\delta k/k$ per gram of material. The sole boron-10 value is the result of several measurements with samples of varying boron-10 content; the value quoted is an extrapolation to zero mass. The calculated values have been normalised to the measured ^{235}U value for each assembly for comparison. As mentioned above, the calculated values are only relative, since no account was taken of the denominator term in the perturbation expression for $\Delta\rho$.

Examination of Table 29 shows that the agreement between theory and experiment varies rather widely. For ^{238}U, for example, there is less than a factor of two in each case between measured and calculated values, whereas for some other materials there is an order of magnitude difference. Some of these discrepancies are certainly due to experimental error, since it is known that the pneumatic oscillator did not function correctly during its use on Assembly 4. Assembly 3 results, as presented, were actually derived from a rebuilt version of this assembly, and benefited from the experience gained on seven or eight earlier sets of measurements.

As previously mentioned, the performance of these reactivity measurements was always regarded as a trial of techniques, and not as an exercise in obtaining few-percent-type agreement with calculation. The results shown, and the extent of agreement reached, are thus regarded as quite satisfactory, and as justification of the methods used for both measurement and calculation.

11. CONCLUSIONS

The quantity of fuel and other material constituents required for reactors has become a limiting factor in their experimental study. The need for a wider range of measurements has forced the use of critical rather than exponential assemblies. It has become common practice to attempt to predict the properties of a reactor from measurements on a two region reactor, the inner region having the composition of the reactor whose properties are being sought.

The study reported here was designed to predict the properties of reactors from measurements made on a 1 ft cube positioned within the two core tanks of the Argonaut type reactor MOATA.

The spacing between MOATA's core tanks (18 inches) precluded the establishment of the core equilibrium spectrum. The situation was further aggravated by the need to have large diameter holes (1 inch and 2 inches) through the assembly for reactivity, activation and fission chamber measurements. Under these conditions the object of the experiment became the calculation of the measured properties.

Prediction of the properties of two-tank heterogeneous reactors (e.g. MOATA) is difficult. It is difficult to construct two dimensional models which are physically realistic in detail. This is particularly so even in the model considered for the representation of the light water reflector above and below the fuel elements. The widely differing properties of graphite and light water make suitable homogenisation difficult. The model used, while having several ad hoc features, was considered to be quite successful on most counts.

Despite uncertainty as to whether an asymptotic spectrum had been achieved within the assembly, the results indicate substantial agreement between measured and calculated quantities. The measure of agreement obtained generated some confidence in the methods (both experimental and calculational) and nuclear data used. Analysis indicated that greater attention to detail is required in this approach to reactor physics if confidence is to be placed in using the methods and data for assessing reactors of the same composition. More attention to detail might have improved the agreement between measurement and calculation, but general considerations suggest that current discrepancies could be offset against the model, the nuclear data or calculational method used, just as easily as against the measurements.

Although comparison of measured values with predictions is valuable for assessing the ability to predict reactor properties, there is no doubt that a measurement of the critical mass of the reactor would be accorded a higher weighting than most of the measurements actually made. The measurements made, though valuable, are not as sensitive to changes in the data and methods as one would have liked.

The programme has shown that two-region experiments using relatively small amounts of material conforming to reactor composition can be used successfully to provide data for a reasonable production of reactor properties. More confidence would be generated if a critical mass comparison were available.

12. ACKNOWLEDGEMENTS

This series of measurements and calculations has been notable for the degree of assistance and collaboration required, and given, for its completion.

Separate reports on particular aspects of the work have been published by Dr. R. B. Tattersall, Dr. A. W. Dalton and Messrs. J. W. Connolly, T. Wall and A. Rose. The author is grateful for their participation in this work.

The author also wishes to express his appreciation to:

Mr. J. P. Sawyer and Mr. R. Jones (for valuable assistance in operation of MOATA),

Mr. G. K. Brown (for design and construction of much experimental equipment and for assistance in its operation),

Mr. P. Duerden (for assistance in carrying out measurements),

Mr. J. P. Pollard (for advice and assistance freely given in connection with calculations),

Mr. P. Ellis (for construction and modification of digital equipment).

The work was unquestionably a group effort and could not have been completed without the help of many other members of Experimental Physics and Theoretical Physics Sections, General Physics Section, (counting techniques and general electronics), Materials Division (production of special materials including BeO and uranium foils), and members of MOATA operating staff (for patient and painstaking assistance in building the assemblies and carrying out the measurements).

13. REFERENCES

Connolly, L.D. (1963). – Los Alamos group averaged cross sections LAMS–2941.

Connolly, J.W., Rose, A. and Wall, T. (1963). – Integral reaction rates and neutron energy spectra in a well moderated reactor. AAEC/TM191.

Connolly, J.W., Wall, T. and Rose, A. (1968). – A resonance self-screening technique for the measurement of epithermal-neutron spectra. Nucl. Applications, 4: 31.

Cripps, P.B. (1969). – Theoretical calculations and comparison with experimental results on BeO-^{235}U and BeO-Th-^{235}U assemblies at the centre of a low power reactor. AAEC/TM496.

Dalton, A.W. (1969). – The measurement and theoretical analysis of neutron energy spectra in slab lattices of multiplying media. AAEC/TM497.

Doherty, G. (1968). – Theoretical analysis of some heavy water natural uranium lattices. AAEC/TM461.

Duerden, P., McCulloch, D.B. and Brittliff, E. (1964). – Buckling and integral spectrum measurements in ^{235}U/BeO subcritical assemblies. AAEC/E123.

Ellis, P.J. (1967). – Digital voltmeter read-out system type 173. AAEC/M74.

Francescon, S. (1963). – The Winfrith DSN programme. AEEW-R273.

Hassitt, A. (1962). – A computer programme to solve the multigroup diffusion equations. TRG Report 229(R).

Hogan, W.S. (1960). – Negative-reactivity measurements. Nucl. Sci. & Eng. 8: 518.

Keepin, G.R. (1965). – Physics of Nuclear Kinetics. Addison-Wesley Publishing Co. Inc. Reading, Mass.

McGregor, B., Richards, A.G. and Wood, R.G.J. (1968). – An IBM 360 version of the neutron diffusion code CRAM. AAEC/TM429.

Marks, A.P. (1962). – MOATA reactor. Atomic Energy in Australia, 5 (4): 9.

Pollard, J.P. and Robinson, G.S. (1966). – GYMEA – A nuclide depletion, space independent, multigroup neutron diffusion data preparation code. AAEC/E147.

Spinks, N. (1967). – Worth of boron rod in the reactor MOATA. AAEC/E181.

Tattersall, R. B. (1967a). – Methods used to analyse experimental data obtained with the MOATA time-of-flight analyser. AAEC/E169.

Tattersall, R.B. (1967b). – Differential neutron energy spectrum measurements on ^{233}U/BeO and ^{235}U/BeO assemblies in the reactor MOATA. AAEC/E171.

APPENDIX 1

DETAILS OF LOADING ARRANGEMENTS FOR ASSEMBLIES

In each case, details are given of the contents of successive layers, comprising BeO, Al and ^{235}U foils. These are set out here in the same way as the actual loadings, i.e. lowermost layer at the bottom. BeO block types are shown in Figure 2. The layout of foils for each assembly is shown in paragraph A1.6.

A1.1 Assembly 1

A1.1.1 Full box

4 Type E blocks
2 foils
4 Type E blocks } 10 times

A1.1.2 Chopper channel

4 Type E blocks
2 foils
4 Type E blocks } 4 times

2 foils
Al channel spacer, 8 Type A, 8 Type C, 8 Type F, 3 Type G blocks

2 foils
4 Type E blocks } 5 times

16 half-thickness Type A blocks (½ inch thick)

A1.1.3 2 inch Tube

1/16 inch Al sheet (12 inches square)
4 Type E blocks
2 foils
4 Type E blocks } 3 times

2 foils
8 Type A, 8 Type B blocks
1/16 inch Al sheet (2 sheets 0.060 inch x 4½ inch x 12 inch)
2 foils
2 inch tube, 8 Type A, 8 Type C blocks
Al sheet (2 sheets 0.030 inch x 4½ inch x 12 inch)
2 foils
8 Type A, 8 Type B blocks
2 foils
4 Type E blocks } 4 times

7/16 inch Al sheets (12 inch square)

A1.2 Assembly 2

A1.2.1 Full box

4 Type E blocks
3 foils
1/16 inch Al sheet (12 inch square) } 10 times
4 Type E blocks

3/16 inch Al sheets (12 inch square)

APPENDIX 1 (continued)

A1.2.2 Chopper channel

1/16 inch Al sheet (12 inch square)
4 Type E blocks
3 foils
1/16 inch Al sheet (12 inch square) } 4 times
4 Type E blocks

3 foils
1/16 inch Al sheet (12 inch square)
Al channel spacer, 8 Type A, 8 Type C, 8 Type F, 3 Type G blocks

3 foils
1/16 inch Al sheet (12 inch square) } 5 times
4 Type E blocks

1/16 inch Al sheet (12 inch square)

A1.2.3 2 inch Tube

1/16 inch Al sheet (12 inch square)
4 Type E blocks
3 foils
1/16 inch Al sheet (12 inch square) } 3 times
4 Type E blocks

3 foils
1/16 inch Al sheet (12 inch square)
8 Type A, 8 Type B blocks
Al sheet (2 sheets 0.030 inch x 4½ inch x 12 inch)
2 foils
1/16 inch Al sheet (2 sheets 0.060 inch x 4½ inch x 12 inch)
2 inch tube, 8 Type A, 8 Type C blocks
2 foils
1/16 inch Al sheet (2 sheets 0.060 inch x 4½ inch x 12 inch)
8 Type A, 8 Type B blocks
3 foils
1/16 inch Al sheet (12 inch square) } 4 times
4 Type E blocks

1/16 inch Al sheet (12 inch square)

A1.3 Assembly 3

A1.3.1 Full box

1/16 inch Al sheet (12 inch square)
4 Type E blocks
6 foils
1/16 inch Al sheet (12 inch square) } 4 times
4 Type E blocks

6 foils
1/16 inch Al sheet (12 inch square)
8 Type A, 8 Type C, 8 Type F, 6 Type G blocks
6 foils
1/16 inch Al sheet (12 inch square) } 5 times
4 Type E blocks

1/16 inch Al sheet

A1.3.2 Chopper channel

1/16 inch Al sheet (12 inch square)
4 Type E blocks
6 foils
1/16 inch Al sheet (12 inch square) } 4 times
4 Type E blocks

6 foils
1/16 inch Al sheet (12 inch square)
Al channel spacer, 8 Type A, 8 Type C, 8 Type F, 3 Type G blocks

6 foils
1/16 inch Al sheet (12 inch square) } 5 times
4 Type E blocks

1/16 inch Al sheet

A1.3.3 2 inch Tube

This is exactly as in A1.2.3, except:

6 foils instead of 3 foils
4 foils instead of 2 foils

A1.3.4 1 inch Tube

1/16 inch Al sheet (12 inch square)
4 Type E blocks
6 foils
1/16 inch Al sheet (12 inch square) } 3 times
4 Type E blocks

6 foils
1/16 inch Al sheet (12 inch square)
8 Type A, 8 Type D blocks
Al sheet (2 sheets 0.030 inch x 4½ inch x 12 inch)
4 foils
1/16 inch Al sheet (2 sheets 0.060 inch x 4½ inch x 12 inch)
1 inch tube, 8 Type A, 8 Type C, 8 Type F blocks
4 foils
1/16 inch Al sheet (2 sheets 0.060 inch x 4½ inch x 12 inch)
8 Type A, 8 Type D blocks
6 foils
1/16 inch Al sheet (12 inch square) } 4 times
4 Type E blocks

1/16 inch Al sheet (12 inch square)

A1.4 Assembly 4

A1.4.1 Full box

This is exactly as in A1.3.1, except:

12 foils instead of 6 foils

A1.4.2 Chopper channel

This is exactly as in A1.3.2, except:

12 foils instead of 6 foils.

A1.4.3 2 inch Tube

This is exactly as in A1.2.3, except:

12 foils instead of 3 foils
6 foils instead of 2 foils

A1.4.4 1 inch Tube

This is exactly as in A1.3.4, except:

12 foils instead of 6 foils
6 foils instead of 4 foils

A1.5 Assembly 5

A1.5.1 Full box

This is exactly as in A1.3.1, except:

18 foils instead of 6 foils

A1.5.2 Chopper channel

This is exactly as in A1.3.2, except:

18 foils instead of 6 foils

A1.5.3 2 inch Tube

This is exactly as in A1.2.3, except:

18 foils instead of 3 foils

12 foils instead of 2 foils

A1.5.4 1 inch Tube

This is exactly as in A1.3.4, except:

18 foils instead of 6 foils
12 foils instead of 4 foils

A1.6 Foil Layout

The following diagrams show the disposition of uranium foils in each 12 inch square layer. For Assembly 1, the foils were manually placed in approximately the positions shown. For all subsequent assemblies, the foils were attached to 12 inch square Al sheets, as already described.

Foils omitted in tube arrangements (two central layers only) are shown with double hatching.

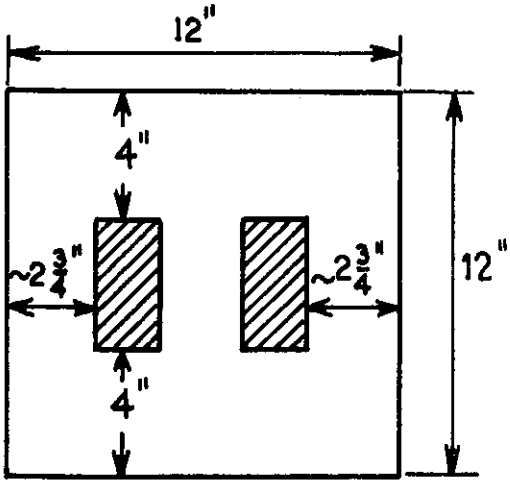

Assembly 1
(2 foils/layer)

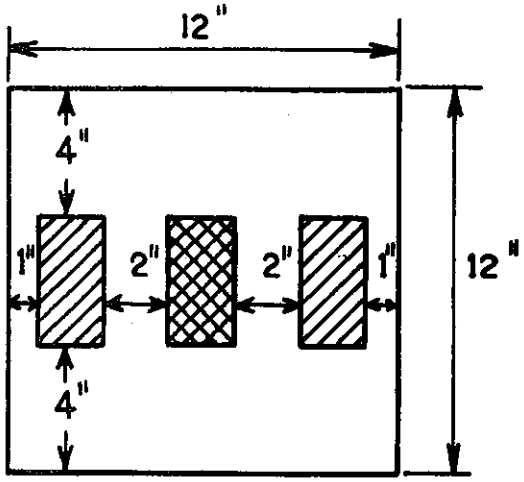

Assembly 2
(2 foils/layer)

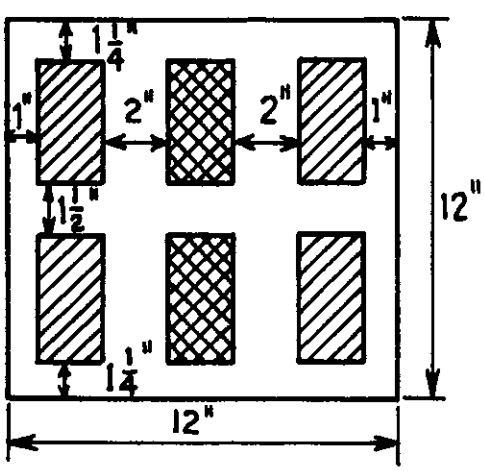

Assembly 3
(6 foils/layer)

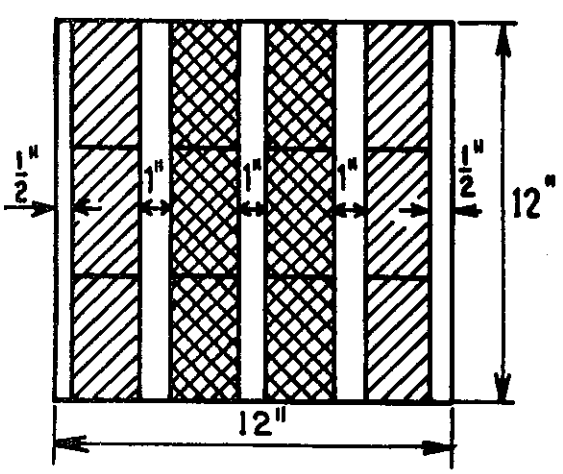

Assembly 4
(12 foils/layer)

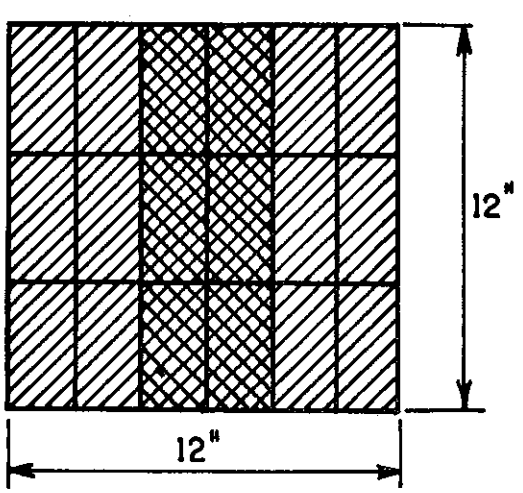

Assembly 5
(18 foils/layer)

APPENDIX 2

CALIBRATION OF ^{233}U CHAMBER

Isotope	Assay	Mass per μg total	Specific Activity d/sec/μg	Decay Rate d/sec
^{232}U	10.8 p.p.m.	1.08×10^{-5}	7.75×10^{5}	8.37
^{233}U	87.87%	8.787×10^{-1}	3.50×10^{2}	307.55
^{234}U	0.83%	8.3×10^{-3}	2.28×10^{2}	1.89
^{235}U	0.09%	9×10^{-4}	7.89×10^{-2}	0
^{236}U	<0.03%	$<3 \times 10^{-4}$	2.34	0
^{238}U	11.21%	1.121×10^{-1}	1.23×10^{-2}	0

Total decay rate 317.81 disintegrations/sec/μg.

Measured 2π decay rate 9370 ± 90 disintegrations/sec.

Hence total uranium content is given by

$$\frac{2 \times 9370}{317.81} = 58.97\ \mu g\ .$$

The decay rate was measured by D. Urquhart of General Physics Section, using absolute alpha-counting. The quoted decay rate has already been corrected for dead-time losses (dead-time was 3 μ sec) and for back-scattering (2 percent). The back-scattering correction could be in error by 1 percent, adding a fixed error of that amount to the final result.

No information was available on contamination by non-uranium isotopes, such as thorium, which could have contributed to the observed alpha-decay rate. The quoted standard deviation of ± 90 d/sec refers solely to counting statistics.

The decay rate of ^{233}U was known to about 0.5 percent, while the quoted counting statistics gave a 1 percent uncertainty. Hence the standard deviation of the 58.97 μg result was about 1.1 percent, with the additional fixed error of 1 percent due to back-scattering corrections. This gave a combined error of 1.5 percent.

Hence foil content was 58.97 ± 0.88 μg or 58.97 μg ± 1.5 percent.

APPENDIX 3

TREATMENT OF CHART DATA

If the reactor is on an asymptotic period, then the time-voltage response of an ion-chamber output is given by

$$v = v_0 \exp(t/\tau) \quad , \tag{1}$$

where v is the voltage at time t,

v_0 is the voltage at an arbitrary time zero, $t = 0$

and τ is the period, which may be positive or negative.

The basic property of this exponential function is that voltages appear as ratios, while times appear as differences. Hence, provided that the region of asymptotic period is chosen, the zero-time point t_0 may be selected completely arbitrarily. In the present work, it has been assumed that the asymptotic periods involved are sufficiently long for the exponential function to approximate accurately a linear relation.

Thus (1) becomes

$$v = v_0 \ (1 + t/\tau) \quad , \tag{2}$$

and the period is given explicitly by

$$\frac{1}{\tau} = \frac{v - v_0}{(t - t_0) v_0} \quad , \tag{3}$$

where the zero-time t_0 has been introduced, since it is effectively equal to zero.

Thus treatment of chart data consists in selecting values for v, v_0, t and t_0 on the linear portion of each leg to be analysed.

At the power used for most of this work, the d.c. amplifier output voltage was about 20 millivolts, and fluctuations caused by sample movement and the consequent rise and fall of reactor power were from say ± 0.5 millivolts to ±5 millivolts, depending on the sample concerned. Maximum sensitivity to these variations was achieved by backing off the voltage v by a voltage V_B, and displaying the difference $v - V_B = V$ on a scale ranging down to one millivolt full-scale. Thus Equation 3 becomes

$$\frac{1}{\tau} = \frac{V - V_0}{(t - t_0)(V_0 + V_B)} \quad . \tag{4}$$

It was convenient to record V, V_0 as fractions of one millivolt, since recorder charts were calibrated in that way, and to allow for the various recorder ranges by a factor K, where K has possible values 1, 2, 5, 10, 20 corresponding to the various recorder ranges with full-scale sensitivity of 1, 2, 5, 10 and 20 millivolts respectively.

It was also convenient to measure time as a length on the chart, with a knowledge of chart speed S in seconds per division. Thus $t - t_0$ became $S(T - T_0)$, where T, T_0 were measured in chart divisions.

The method of obtaining a back-off voltage in the Kent recorder employed was to set a 10-turn helipot as required. This helipot, which was calibrated from 0.0 to 10.0, actually provided ± 50 millivolts nominal back-off, with a measured zero at the reading 4.92. Hence the actual back-off voltage provided was related to a helipot reading of H by

$$V_B = 10 \ (H - 4.92) \quad .$$

APPENDIX 3 (continued)

We then have the working relationship

$$\frac{1}{\tau} = \frac{K(V-V_o)}{S(T-T_o)\ [KV_o + 10(H-4.92)]} \quad ,$$

for the inverse period, or

$$\tau = \frac{[10(H-4.92) + KV_o]\ S\ (T-T_o)}{K(V-V_o)} \quad . \qquad (5)$$

The values H, K, S, V V_o, T and T_o were recorded for each leg of interest, and Equation (5) evaluated to give the period τ in seconds.

A Fortran programme RCA was written for the IBM 7040 computer, and later adapted for the 360 computer, to evaluate (5) and to give standard listings of results. For a large volume of data this is well worth while, since arithmetical correctness is more readily obtained from a computer than from multiple manual calculations, however elementary.

Data entered into the programme consist of a series of values for 'legs': legs are grouped into 'sequences' if that group of legs is to be averaged together. The averaging method employed by the programme, applied to all data in one sequence, is to sort out all legs for sample 'IN' and all legs for sample 'OUT', the total number of legs being tallied in each case. Then the mean in-leg reactivity $\bar{\rho}_{IN}$ and the mean out-leg reactivity $\bar{\rho}_{OUT}$ are calculated, and the mean sample reactivity found from

$$\bar{\rho} = \bar{\rho}_{IN} - \bar{\rho}_{OUT} \quad .$$

APPENDIX 4

PUNCHED PAPER TAPE RECORDING AND PROCESSING

The punched paper tape which was used to record reactor power fluctuations for the series of reactivity measurements was the five-hole type, punched on a tally tape punch. The code used was the Baudot or teletype code subset with fourteen legal characters, as follows:

Character	Baudot Code					
	5	4	3	S	2	1
0	1	0	1	o	1	0
1	1	0	1	o	1	1
2	1	0	0	o	1	1
3	0	0	0	o	0	1
4	0	1	0	o	1	0
5	1	0	0	o	0	0
6	1	0	1	o	0	1
7	0	0	1	o	1	1
8	0	0	1	o	1	0
9	1	1	0	o	0	0
Decimal Point	1	1	1	o	0	0
Carriage Return	0	1	0	o	0	0
Figures Shift	1	1	0	o	1	1
Space	0	0	1	o	0	0
Minus	0	0	0	o	1	1

where '1' indicates a punched hole

'0' indicates no punched hole

'o' indicates sprocket perforation.

Tape records consisted of Headings and Data. The Heading Record was punched immediately on pressing the start button on the Series 173 equipment, and comprised a two-figure serial number set by thumbwheel switches, plus delineating characters. Data Records were punched at each sampling interval, and comprised an indicator giving sample position IN or OUT, plus the signed digital voltmeter reading, plus delineating characters.

Paper tapes containing such records were read by the IBM 7040–1401 computer, and later by the 360–50H computer, under control of a programme AEPACT (D. J. Richardson, private communication). AEPACT enabled paper tape contents to be converted into punched cards or loaded onto magnetic tape, which was used in this case. In the reading process, the paper tape records were checked for presence of illegal characters, wrong record length, and other errors: the translated records then had a code attached indicating the presence or otherwise of errors and classifying records into headings and data.

Magnetic tape contents were able to be listed by the programme TAPRS; error records revealed on inspection of the listing could then be corrected by the programme CPACT, which created a new magnetic tape in the process. Finally, two magnetic tapes were able to be combined by the programme COMPACT. TAPRS, CPACT, and COMPACT were written by W. J. Turner (private communication).

APPENDIX 5

TREATMENT OF TAPE DATA

A5.1 BASIC EQUATIONS

These data were recorded on punched paper tape in the format described in Appendix 4, and consisted of discrete values of voltages obtained at known regular intervals (the sampling period). In the analysis, the reactor was assumed to be on an asymptotic period, either positive or negative, and it was further assumed that transients, existing when samples changed position, could be eliminated by ignoring data for a selected interval of time after each position change.

Voltages were actually obtained from the output of a d.c. amplifier, and the input current to the amplifier was derived from an ion-chamber. For an asymptotic period, the current time characteristic will be given by

$$i = i_0 \exp(t/\tau) \quad (1)$$

where i is the current at time t, i_0 is an arbitrary current at time zero, and τ is the period.

Taking logarithms, we obtain

$$\ln i = t/\tau + \ln i_0 \quad (2)$$

which represents a straight line of slope $(1/\tau)$, the quantity of interest, based on ordinates (ln i) and abscissae t.

In practice, current i was backed off, or suppressed, by a fixed current I_s, and a more sensitive range, of full-scale deflection I_w, used. Thus if the residual current was I,

$$i = I + I_s$$

and the output voltage V was related to the residual current I by the expression

$$V = I/I_w$$

since a current of I_w would give one volt output for the instrument used (Keithley 415). Thus

$$\ln i = \ln (I + I_s) = \ln (VI_w + I_s) ,$$

which becomes

$$\ln I_w + \ln (V + I_s/I_w) .$$

Equation 2 now becomes

$$\ln (V + I_s/I_w) = t/\tau + \ln i_0 - \ln I_w , \quad (3)$$

and the final two terms may be disregarded from the point of view of finding the slope $1/\tau$. This latter assertion is readily verified by considering the equations for carrying out a linear least-squares fit to the values of $\ln (V + I_s/I_w)$ and t, whence the slope is independent of the existence of a zero or non-zero intercept $\ln i_o - \ln I_w$.

The parameters which have to be provided are thus the suppression current I_s, the working range I_w, the sampling period, and the voltages V. Times t are introduced by the product of the sampling period with the current total number of samples.

If we designate the ordinates $\ln(V + I_s/I_w)$ by values of y, and the abscissae t by values of x, the conventional least squares linear fitting equations give the slope of the line, or the regression coefficient, as

APPENDIX 5 (continued)

$$b' = \frac{\sum_j w_j x'_j y'_j}{\sum_j w_j x'^2_j} \qquad (4)$$

where $x'_j = x_j - \bar{x}$

$y'_j = y_j - \bar{y}$,

$\bar{x} = \sum_j w_j x_j / \sum_j w_j$,

$\bar{y} = \sum_j w_j y_j / \sum_j w_j$,

and where w_j is the weighting factor to be attached to the value x_j (or y_j) as an indication of the expected uncertainty of that value.

A5.2 FLUCTUATIONS

Owing to the statistical nature of the ion-chamber detection process, and even in the absence of any variation in neutron flux seen by the chamber, there will be a fluctuation in the chamber output current. The variance of this current is given by

$$\sigma_i^2 = \frac{q}{2RC} \bar{i} \qquad (5)$$

where $\bar{i}$ is the mean current in amps.

q is the mean charge delivered per pulse,

RC is the time constant of the d.c. amplifier input connected to the ion-chamber.

For a boron coated chamber, q has the value 10^{-14} coulombs per pulse, while for the equipment used in this work RC is about 1 second.

Thus $\sigma_i^2 = 5 \times 10^{-15} \bar{i}$. (6)

Take $\bar{i}$ equal to i, the latter given by Equation 1. The quantity recorded and manipulated, and whose fluctuation was required, is V, and the variance of V is given by δ^2 (V).

We have $V = I/I_w = (i - I_s)/I_w$.

Thus $\delta^2 V = \left(\frac{\partial V}{\partial i} \delta i\right)^2 = \left(\frac{\partial V}{\partial i}\right)^2 \sigma_i^2$ (7)

$$\frac{\partial V}{\partial i} = \frac{1}{I_w} ,$$

giving $\delta^2 V = \sigma_i^2 / I_w^2 = 5 \times 10^{-15} i / I_w^2$.

But $i = VI_w + I_s = I_w (V + I_s/I_w)$

and $\delta^2 V = \frac{5 \times 10^{-15}}{I_w} \left(V + \frac{I_s}{I_w}\right)$.

The fluctuation in the working parameter y is obtained thus

$$y = \ln (V + I_s/I_w)$$

and $\delta^2 y = \left(\frac{\partial y}{\partial V}\right)^2 \delta^2 V$.

APPENDIX 5 (continued)

$$\text{i.e.} \quad \delta^2 y = \frac{\delta^2 V}{(V + I_s/I_w)^2}$$

$$= \frac{5 \times 10^{-15}}{I_w} \times \frac{(V + I_s/I_w)}{(V + I_s/I_w)^2} \, .$$

$$\text{Hence} \quad \delta y = \frac{7.1 \times 10^{-8}}{\sqrt{I_w (V + I_s/I_w)}} \, . \tag{8}$$

δy and $\delta y'$ are equivalent, and the weighting factors w_j are then given by

$$w_j = \frac{1}{(\delta y_j')^2} \, . \tag{9}$$

A5.3 LEAST SQUARES FITTING

Equation 4 gives the expression for the slope of the straight line fitted to the values of x and y. The variance of b', $\sigma_{b'}^2$, is given by

$$\sigma_{b'}^2 = \sum_j \left(\frac{\partial b'}{\partial y_j'} \, \delta y_j' \right)^2 \, ,$$

provided that $\delta x_j' = 0$, $\delta y_j' \neq 0$,

and it may be shown that

$$\sigma_{b'}^2 = \frac{\sum_j (w_j x_j' \, \delta y_j')^2}{(\sum_j w_j x_j'^2)^2} = \frac{1}{\sum_j (x_j'/\delta y_j')^2} \, . \tag{10}$$

Using (9), Equation 4 becomes

$$b' = \frac{\sum_j (x_j' \, y_j' / \delta^2 y_j')}{\sum_j (x_j'/\delta^2 y_j')^2} \, . \tag{11}$$

The goodness-of-fit may be estimated by a calculation of χ^2 per degree of freedom. For n points, this is

$$\chi^2 = \frac{1}{n-2} \sum_j \left(\frac{y_j' - b' x_j'}{\delta y_j'} \right)^2 \, , \tag{12}$$

which has the expected value of unity.

Equations 10, 11, and 12 give the quantities required from the fitting process, namely variance of the slope, the slope itself, and the goodness-of-fit, respectively.

A5.4 ANALYSIS PROGRAMME RAC

A Fortran programme RAC was written for the IBM 7040 computer and later adapted to the 360 computer to handle analysis of data recorded on magnetic tape. The translation from paper to magnetic tape is described in Appendix 4. RAC searches the tape for a particular set of data, and

APPENDIX 5 (continued)

having found it, fits a straight line to the data for each 'leg' (the interval between successive movements of the sample from IN to OUT, or OUT to IN). The slope of the line is then calculated as above.

The method of averaging used in RAC is similar to that used in RCA (see Appendix 3), in that the IN-leg values are averaged together, and the OUT-leg values averaged together, and the average sample worth is given by

$$\bar{\rho} = \bar{\rho}_{IN} - \bar{\rho}_{OUT} .$$

The effect of reactor drifts during part of an otherwise stable run is occasionally to reverse the sign of a particular leg. The programme identifies the presence of such atypical legs, and signals the need for manual checking of the data concerned.

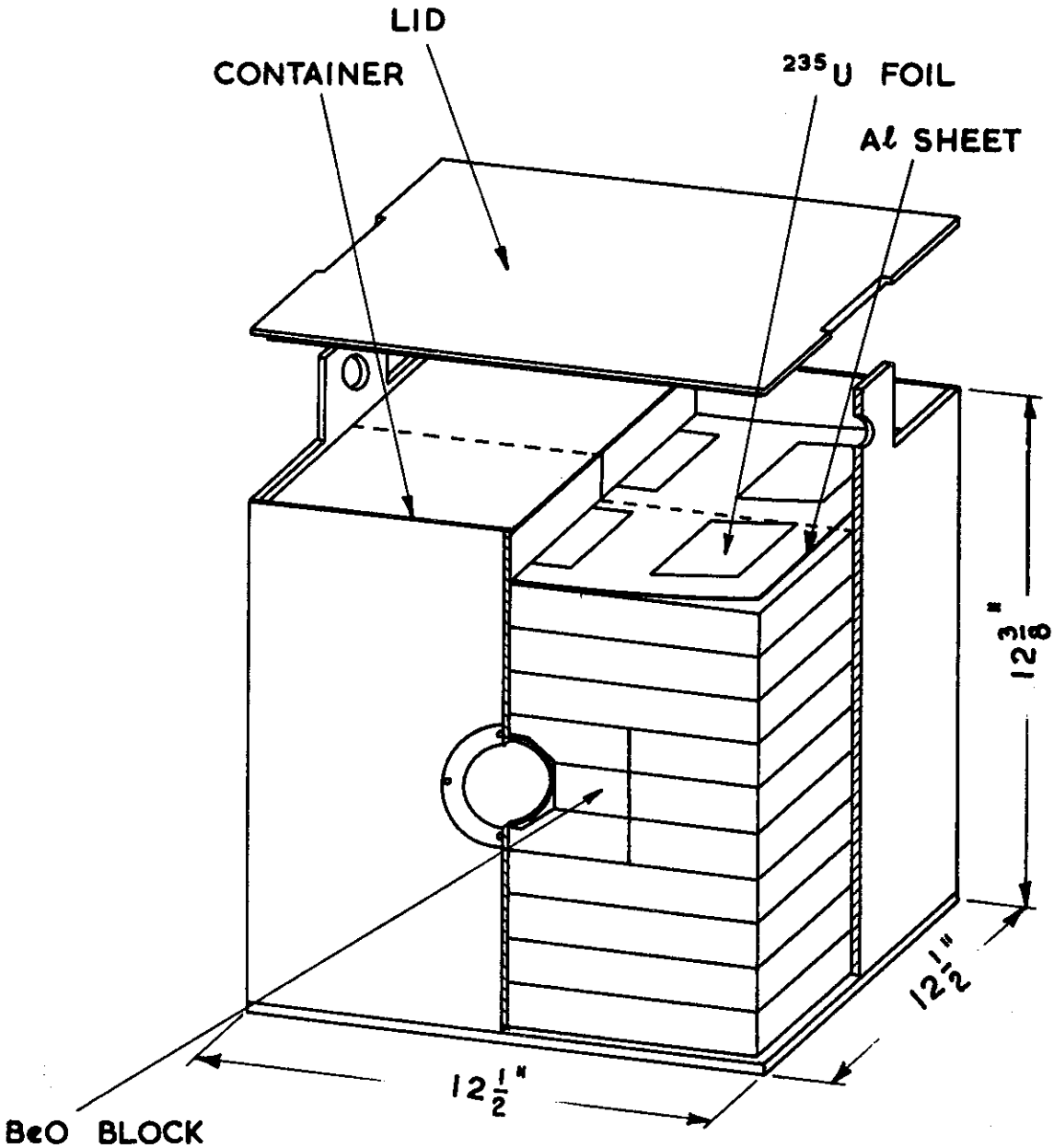

FIGURE 1.

EXPERIMENTAL ASSEMBLY SHOWING BeO/Al/^{235}U LOADING

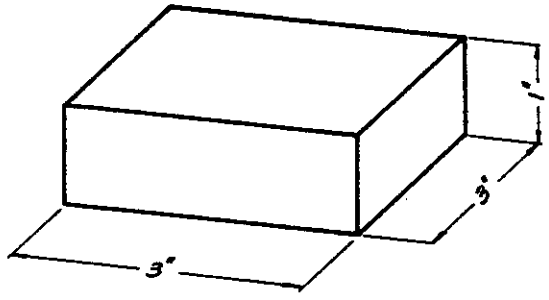

TYPE 'A'

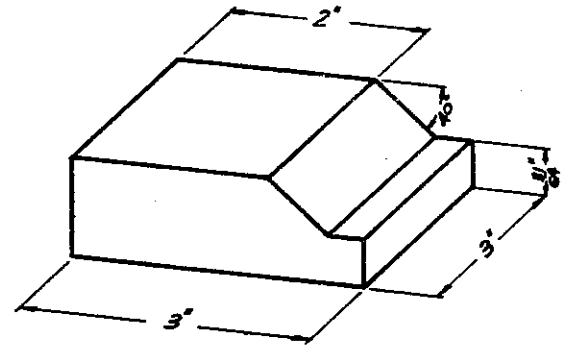

TYPE 'B'

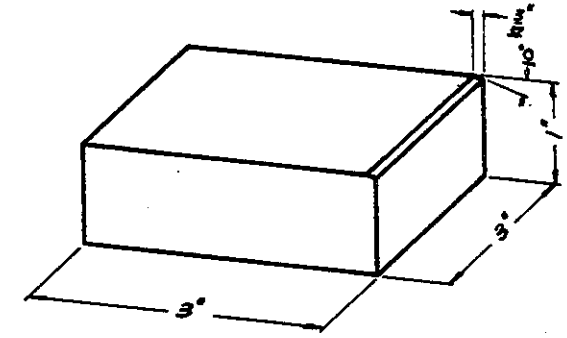

TYPE 'D'

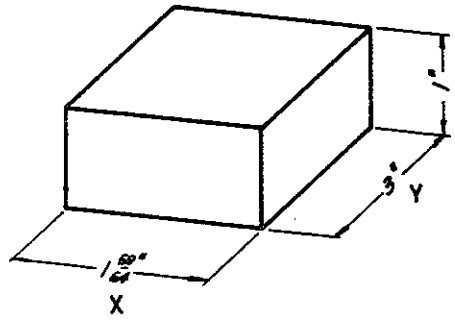

TYPE 'C' & 'G'

	C	G
X	$1\frac{59}{64}$"	1·14"
Y	3"	2"

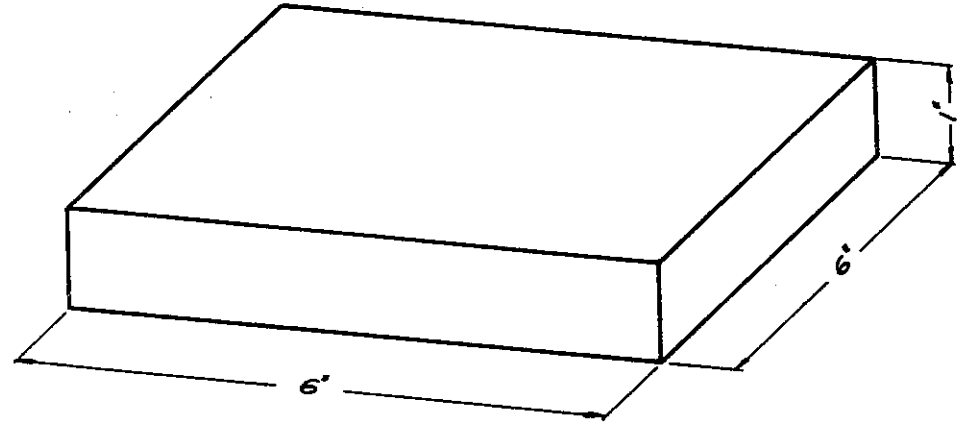

TYPE 'E'

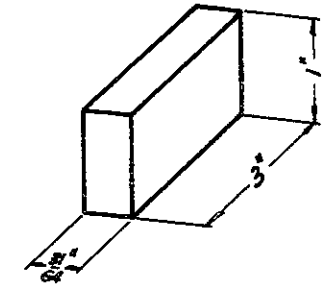

TYPE 'F'

FIGURE 2. TYPES OF BeO BLOCKS

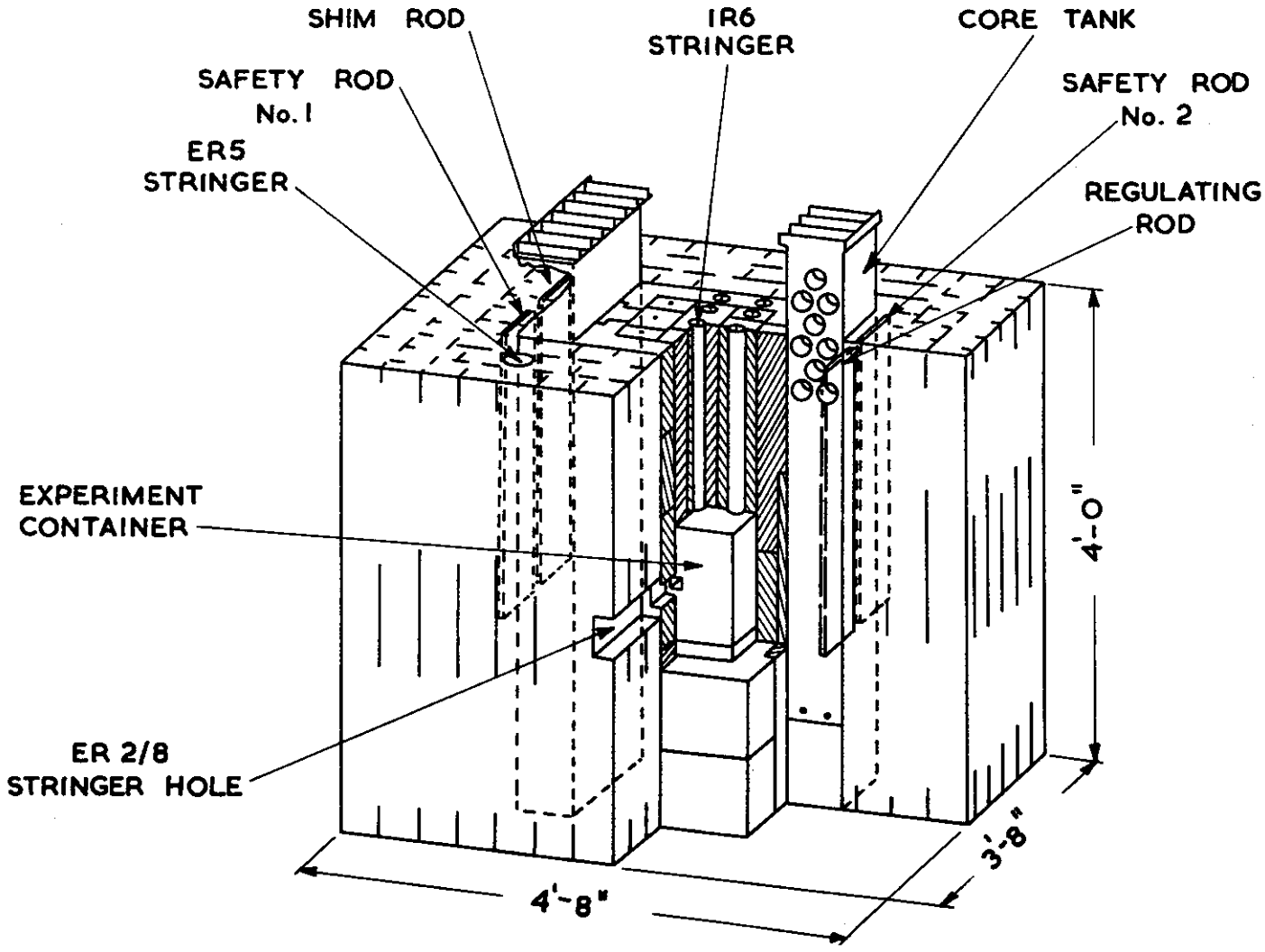

FIGURE 3. MOATA CORE - VIEW ON SOUTH FACE

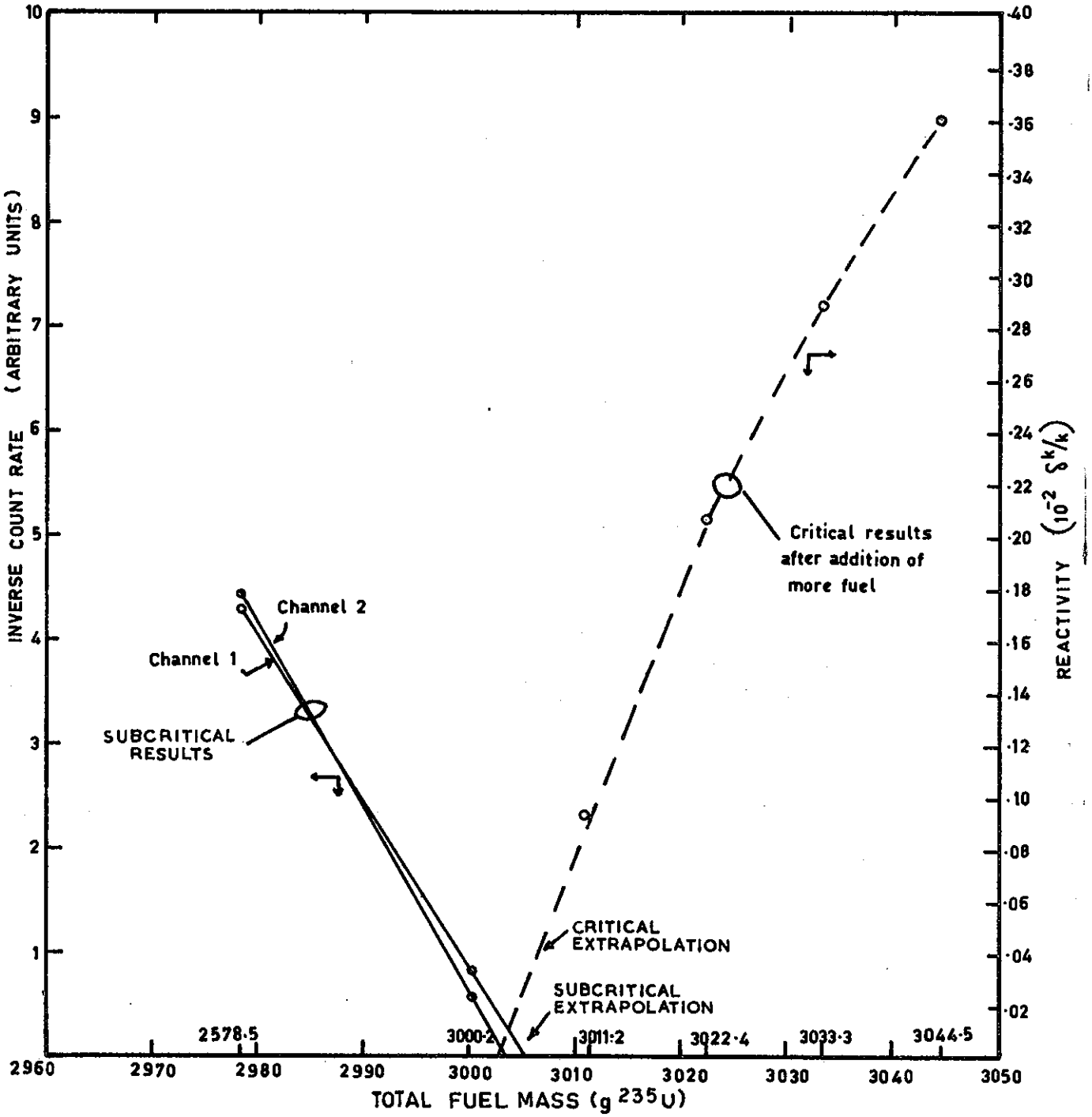

FIGURE 4. CRITICAL MASS - ASSEMBLY 2

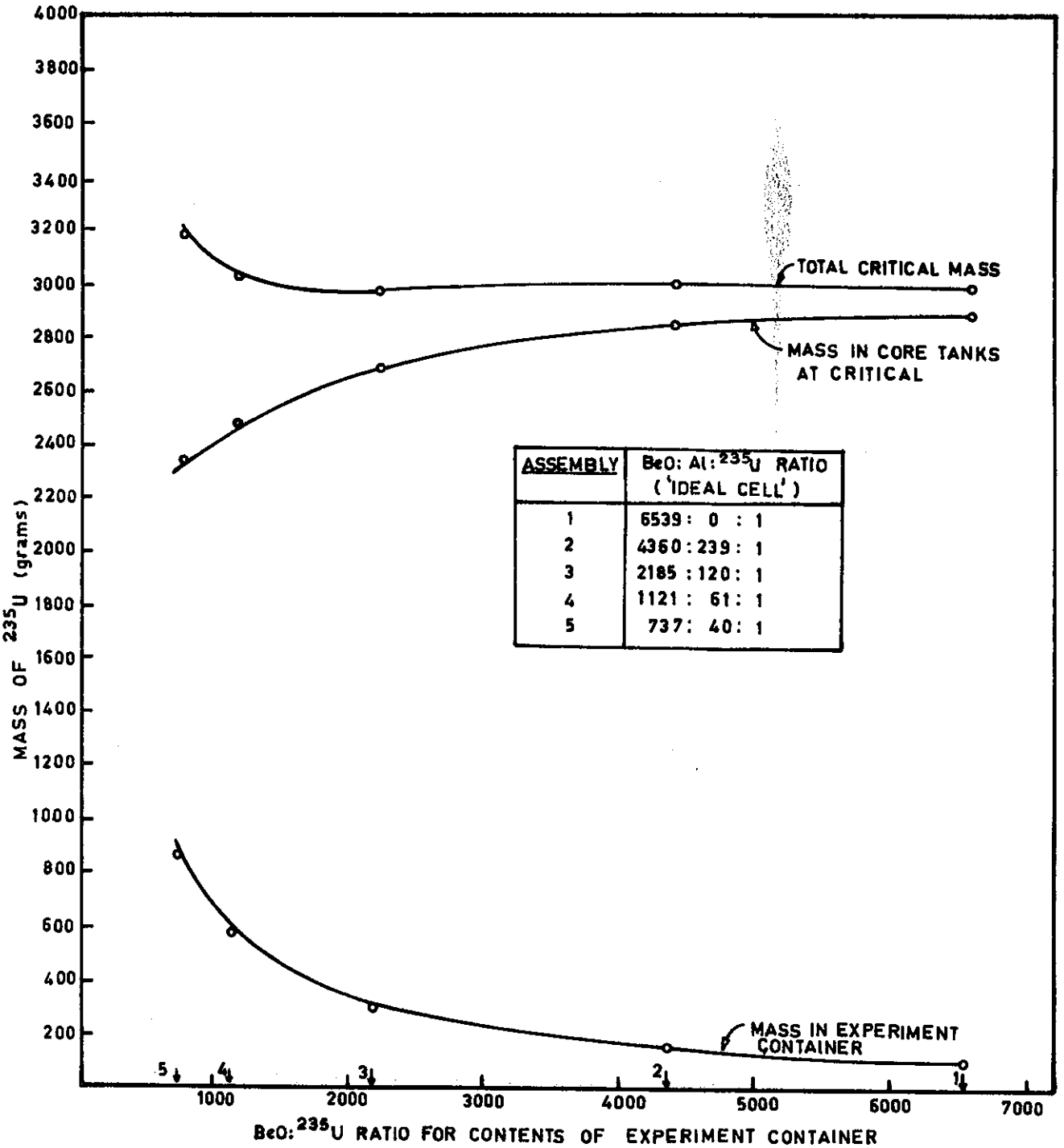

ASSEMBLY	BeO: Al: ^{235}U RATIO ('IDEAL CELL')
1	6539 : 0 : 1
2	4360 : 239 : 1
3	2185 : 120 : 1
4	1121 : 61 : 1
5	737 : 40 : 1

FIGURE 5. CRITICAL MASS AND FUEL LOADING FOR ASSEMBLIES 1 TO 5

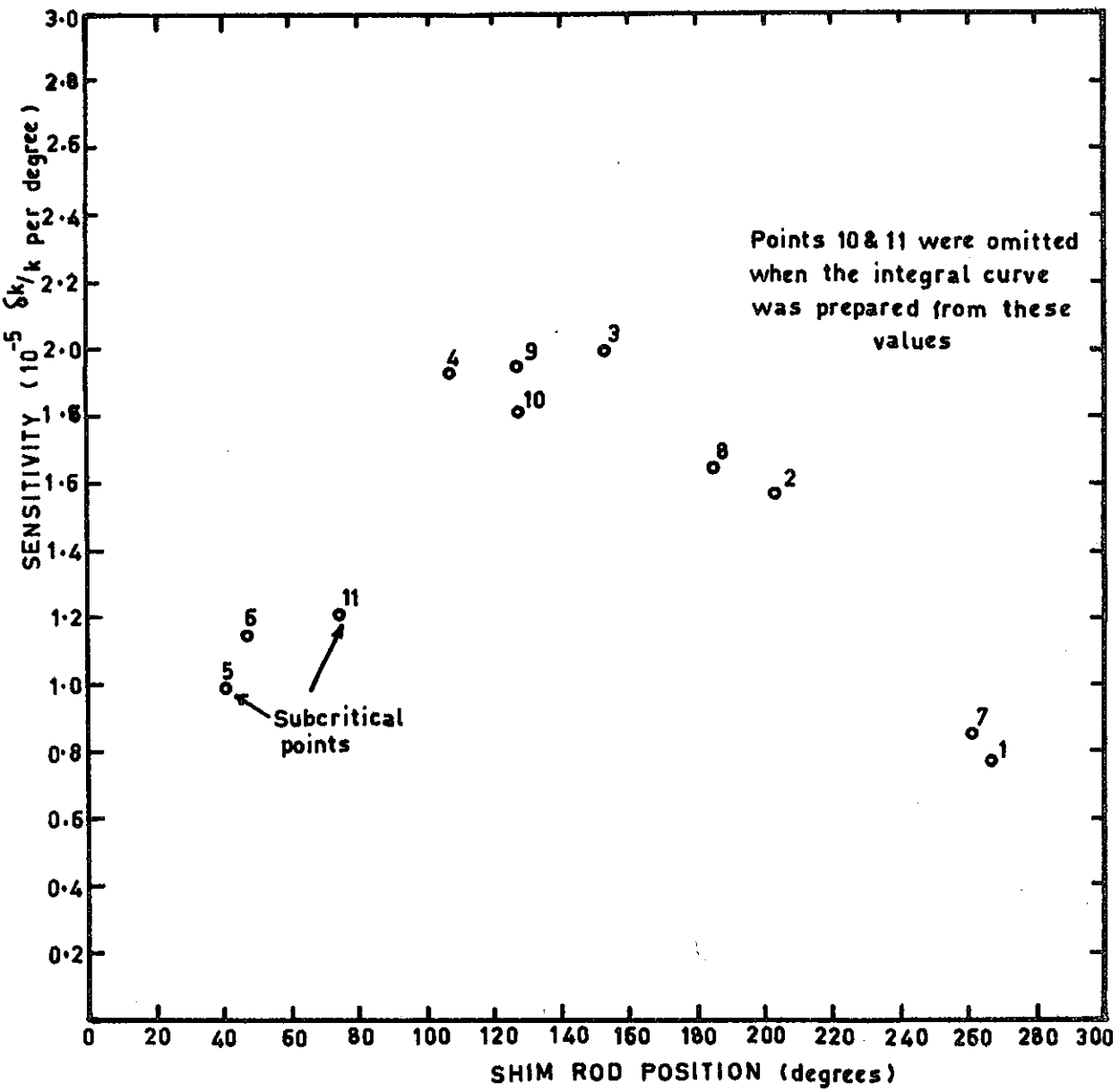

FIGURE 6. SHIM ROD SENSITIVITY VALUES (ASSEMBLY 5)

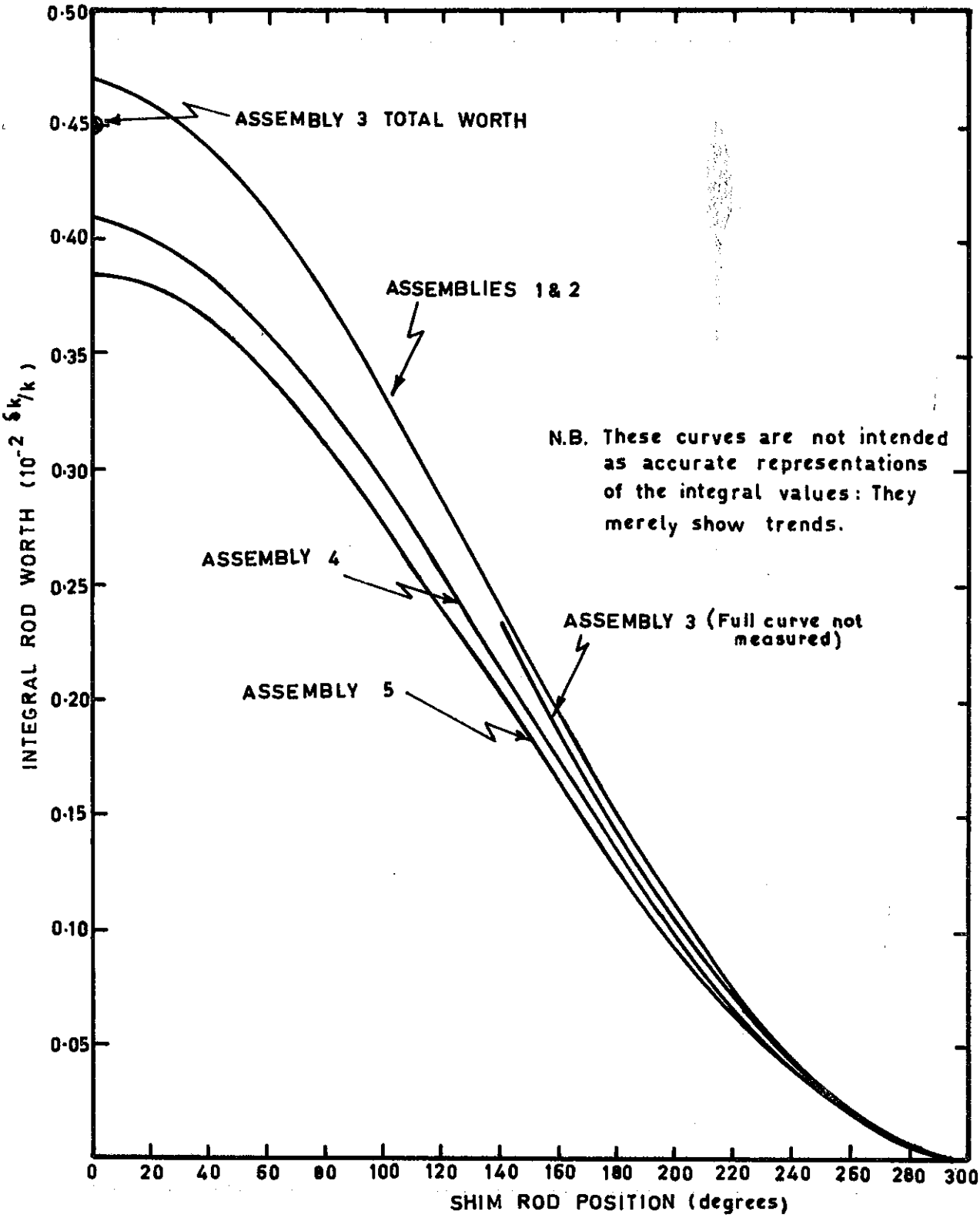

FIGURE 7. SHIM ROD INTEGRAL WORTH

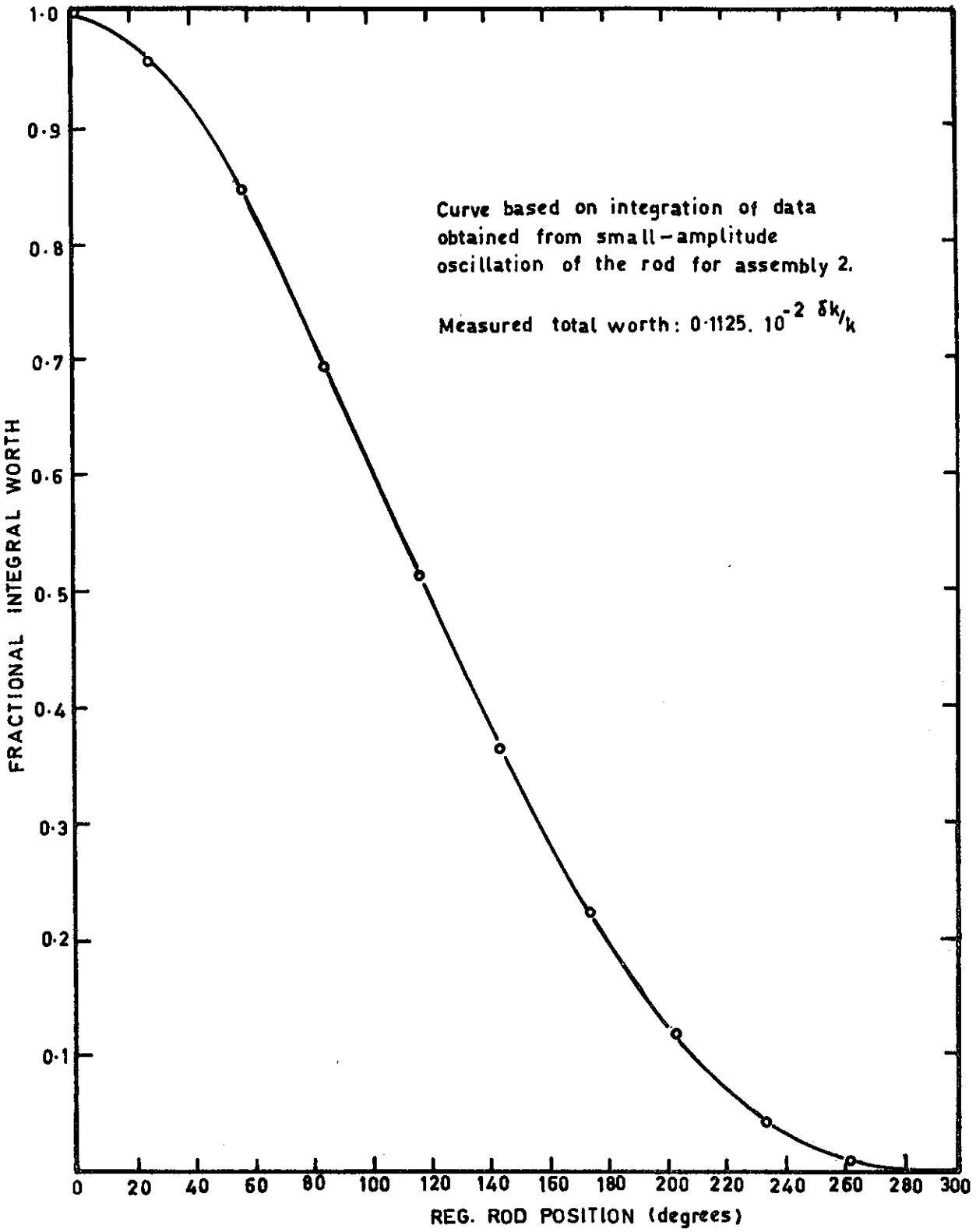

FIGURE 8. REGULATING ROD NORMALISED INTEGRAL WORTH

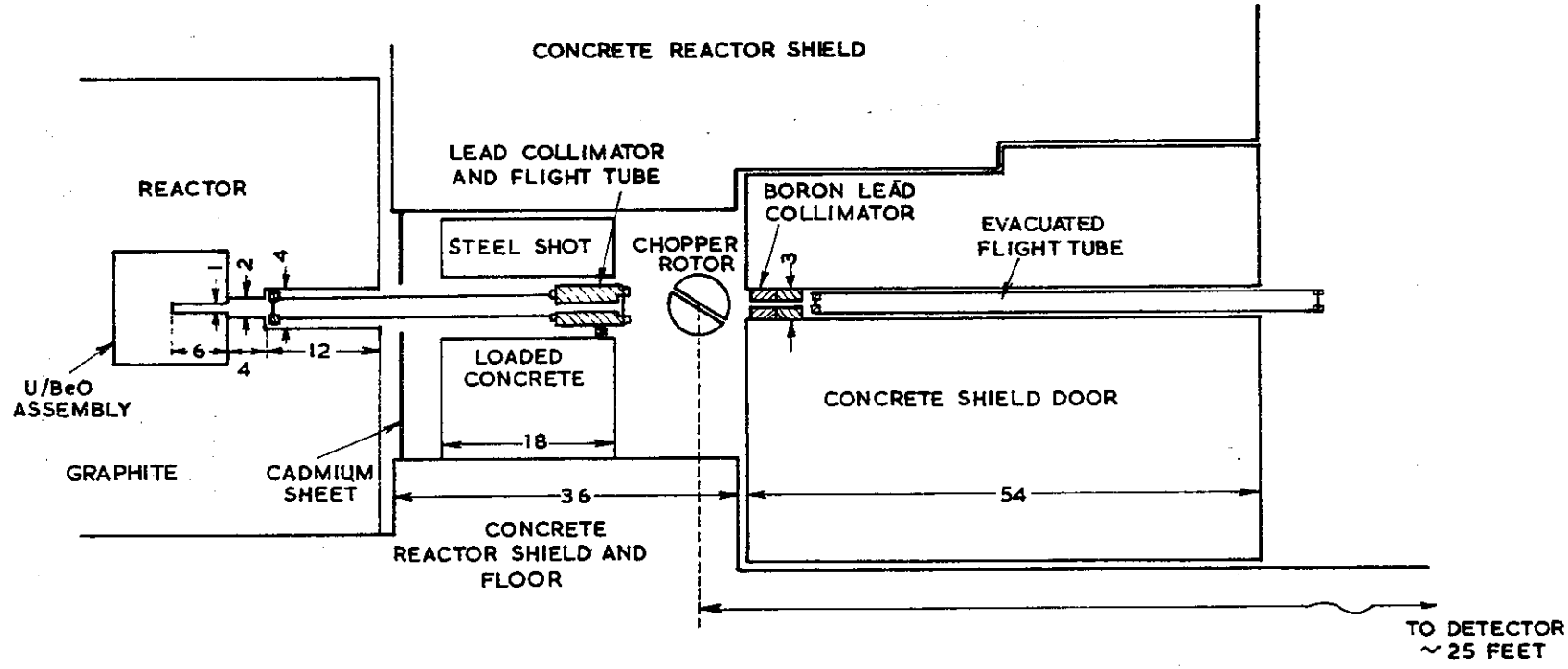

ALL DIMENSIONS IN INCHES

FIGURE 9. TYPICAL COLLIMATOR ARRANGEMENT

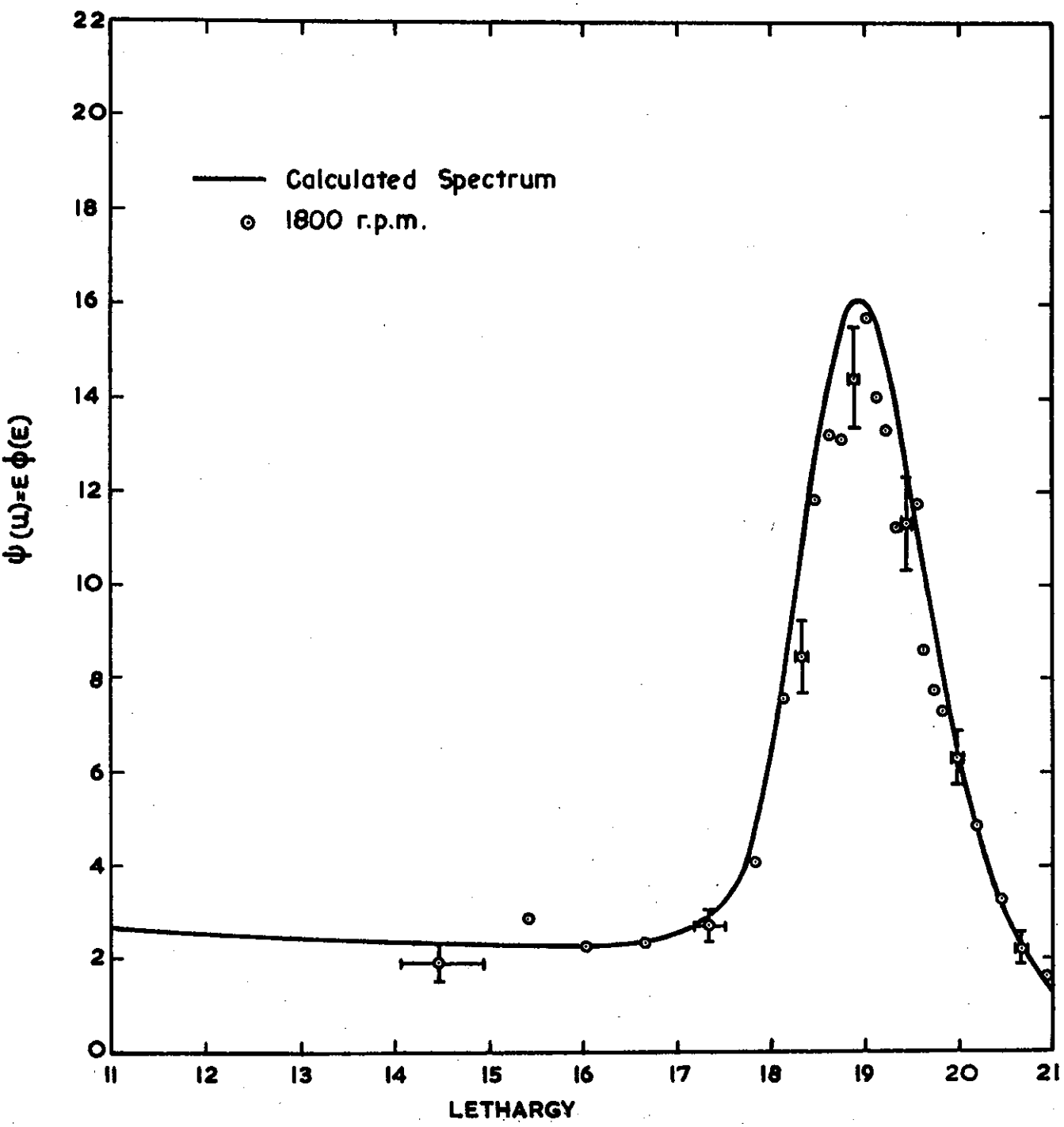

FIGURE 10. SPECTRUM FOR ASSEMBLY 1: $^{235}U/BeO = 1/6545$

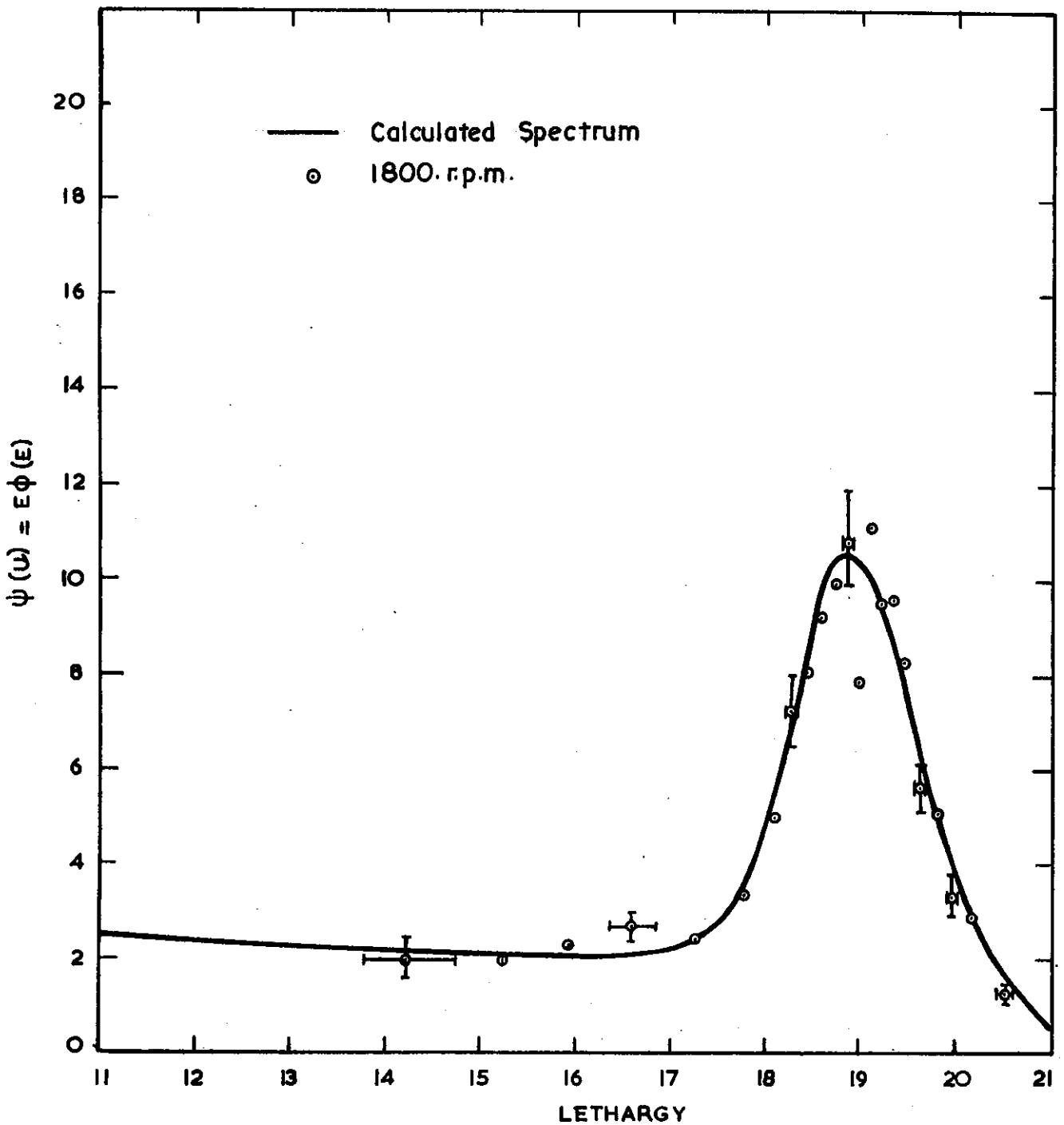

FIGURE 11. SPECTRUM FOR ASSEMBLY 2: ^{235}U/BeO = 1/4360

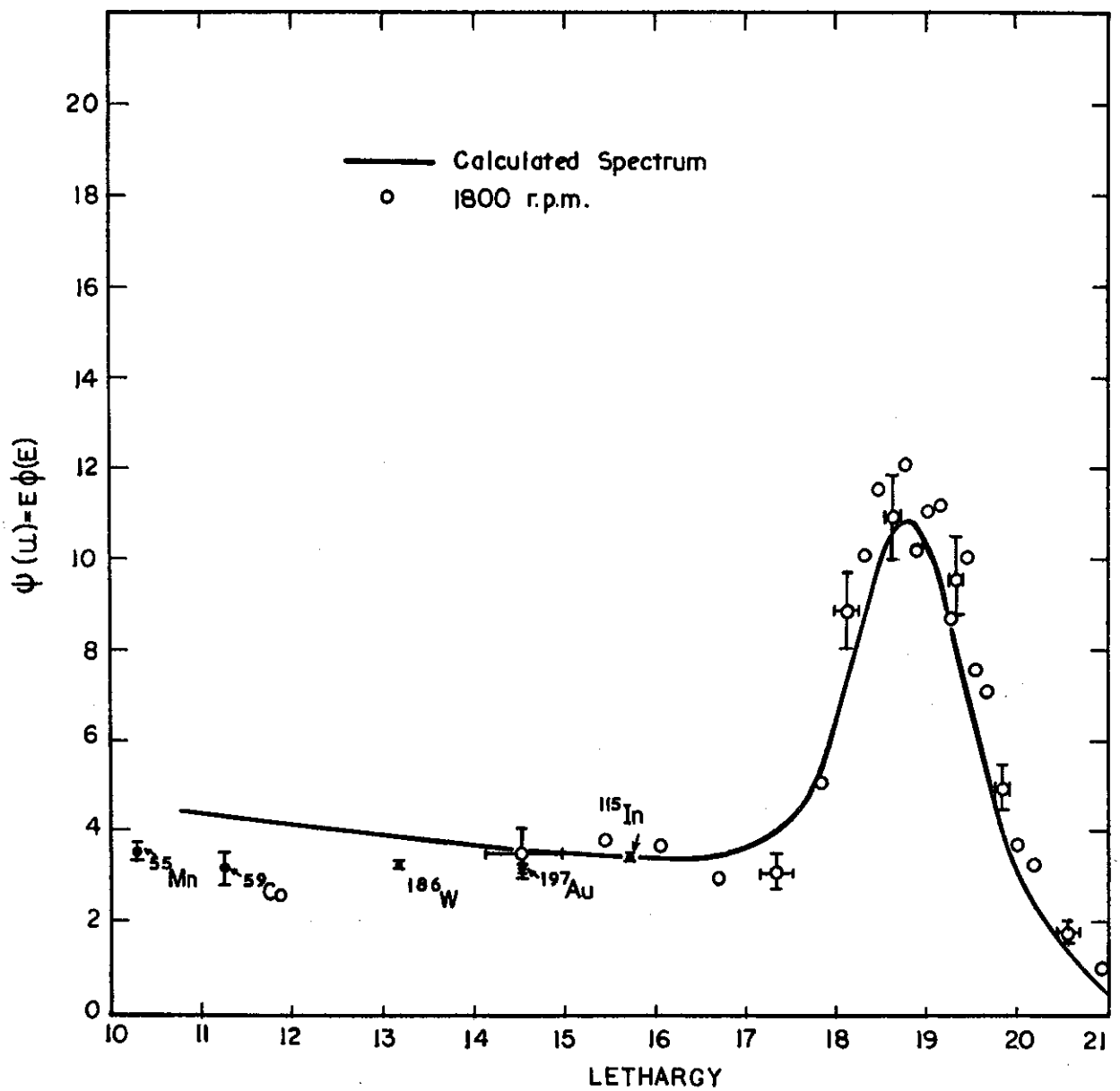

FIGURE 12. SPECTRUM FOR ASSEMBLY 3: $^{235}U/BeO = 1/2185$

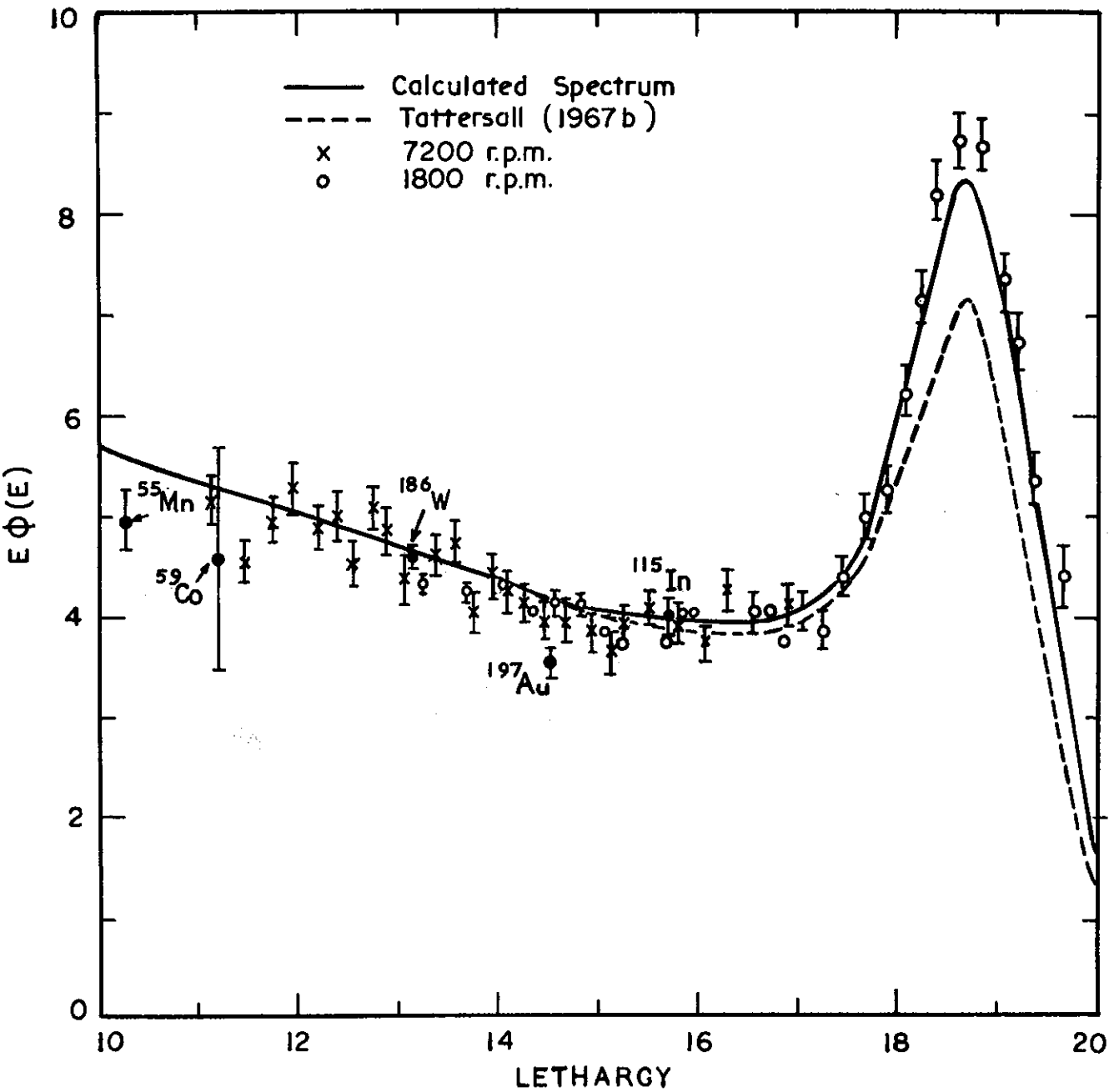

FIGURE 13. SPECTRUM FOR ASSEMBLY 4: ^{235}U/BeO = 1/1120

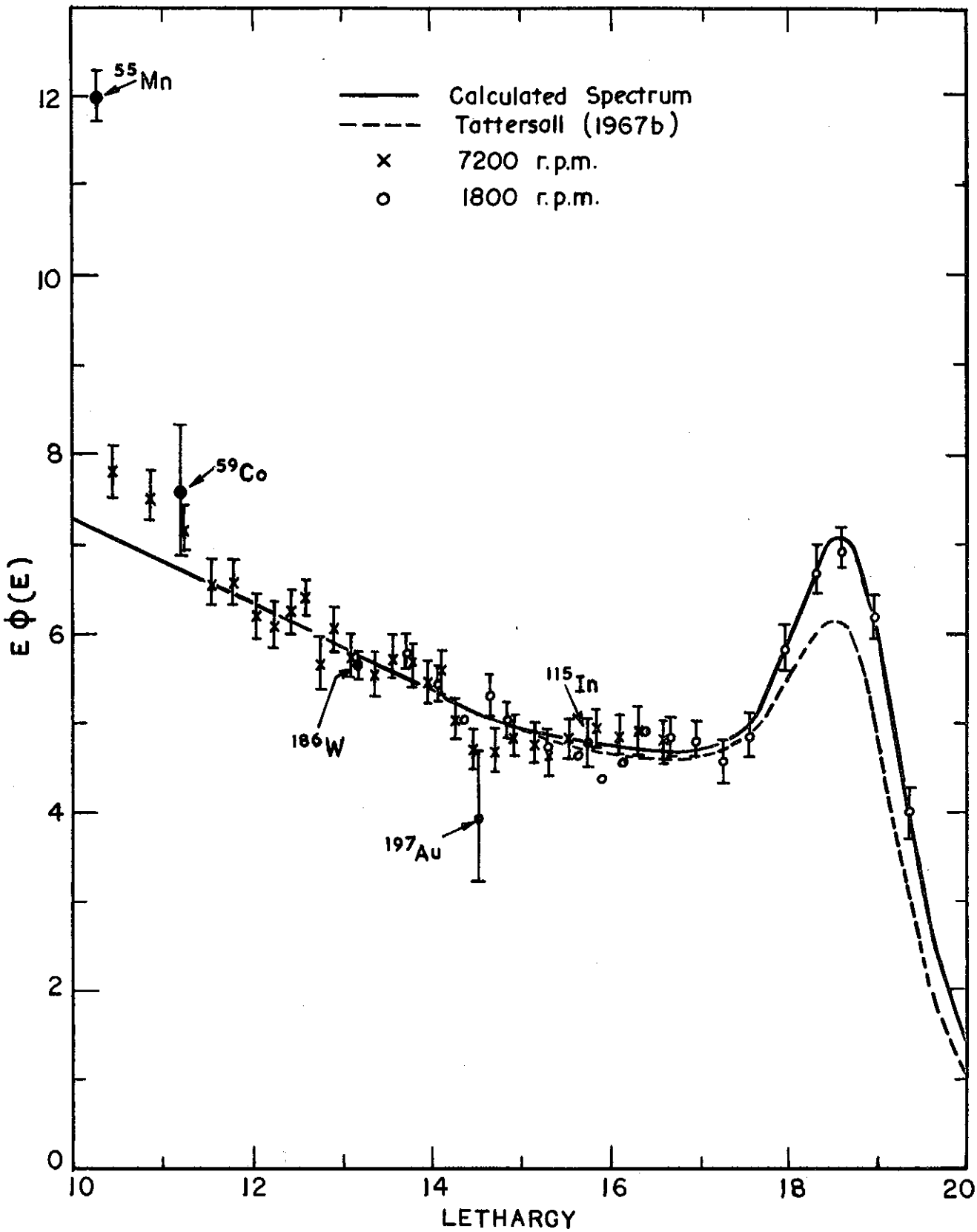

FIGURE 14. SPECTRUM FOR ASSEMBLY 5: ^{235}U/BeO = 1/740

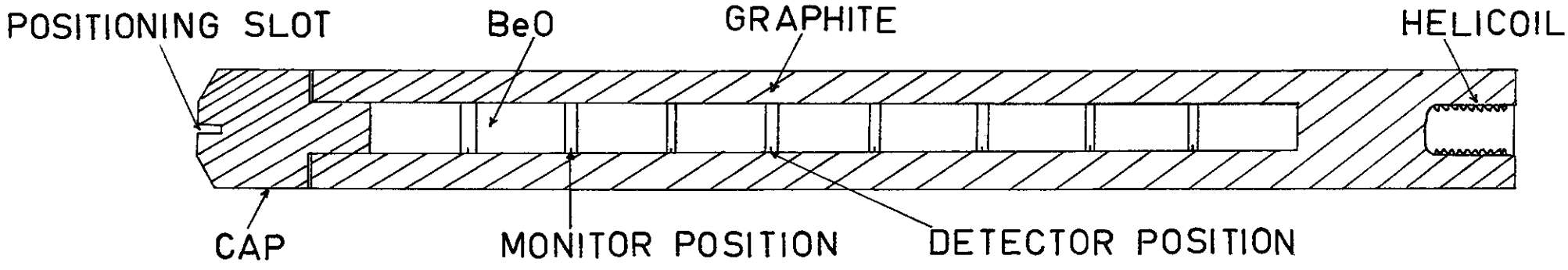

FIGURE 15. DETAIL OF FOIL CARRIER RABBIT

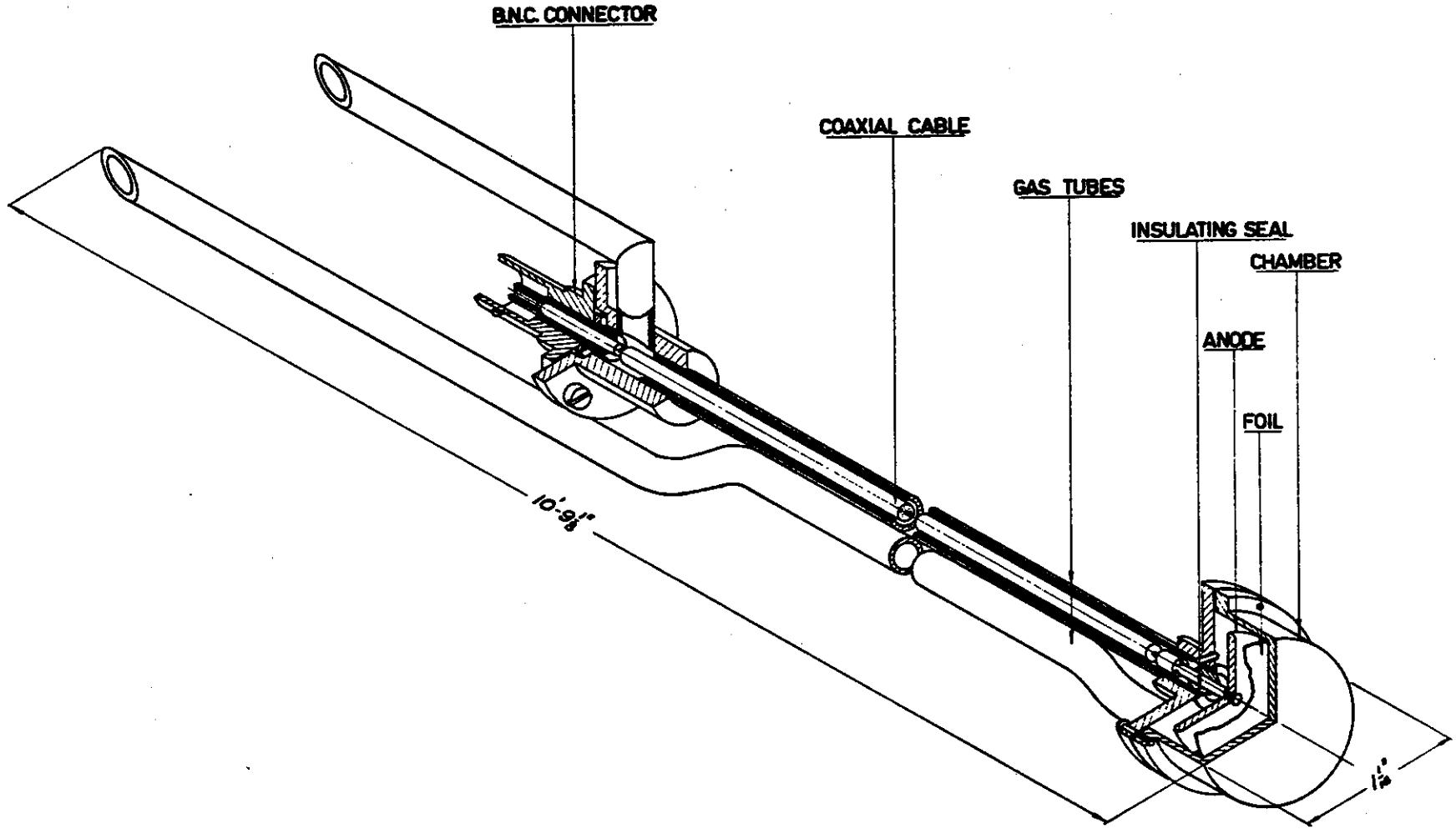

FIGURE 16. GAS FLOW FISSION CHAMBER

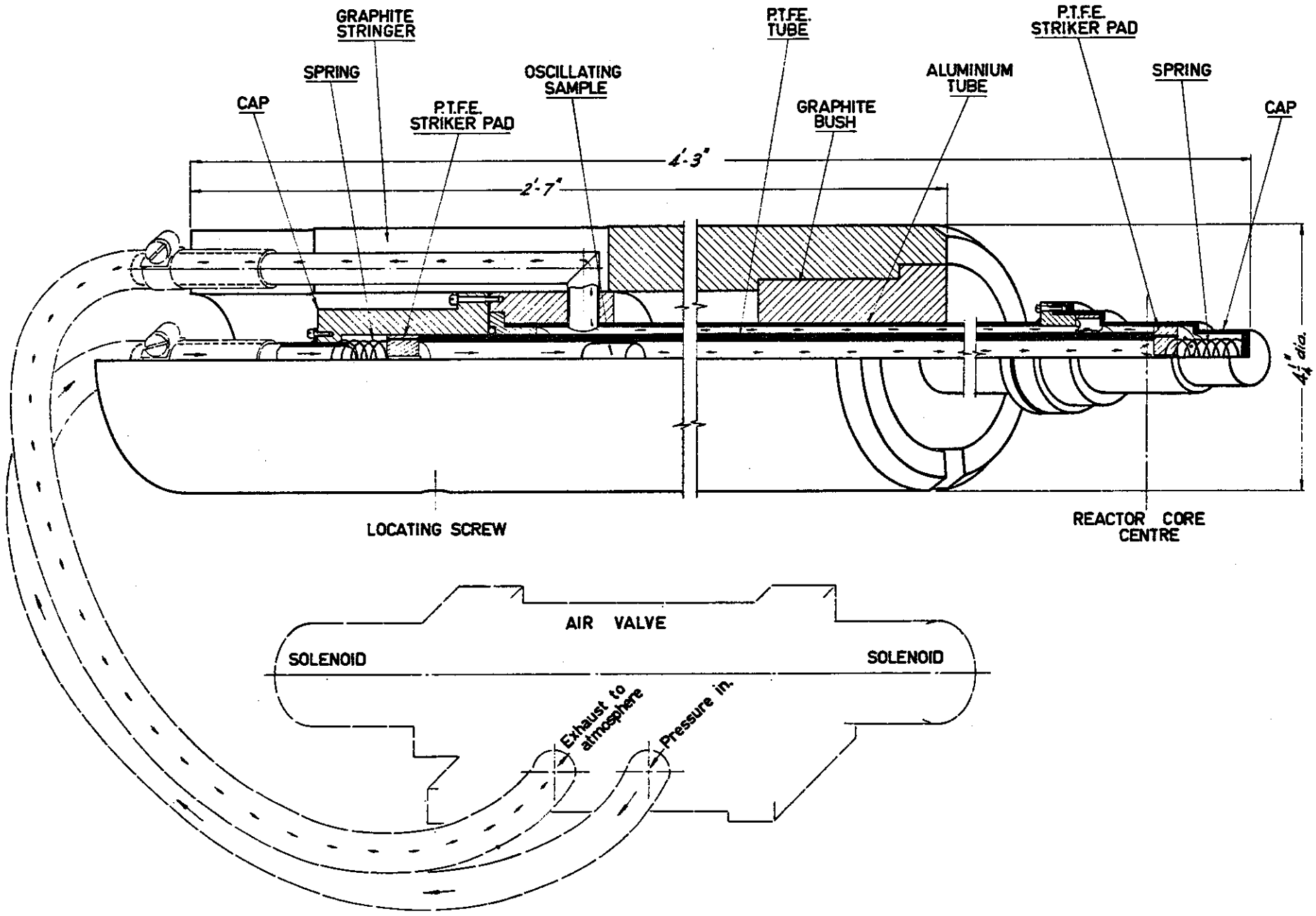

FIGURE 17. MOATA PNEUMATIC OSCILLATOR (Free moving sample)

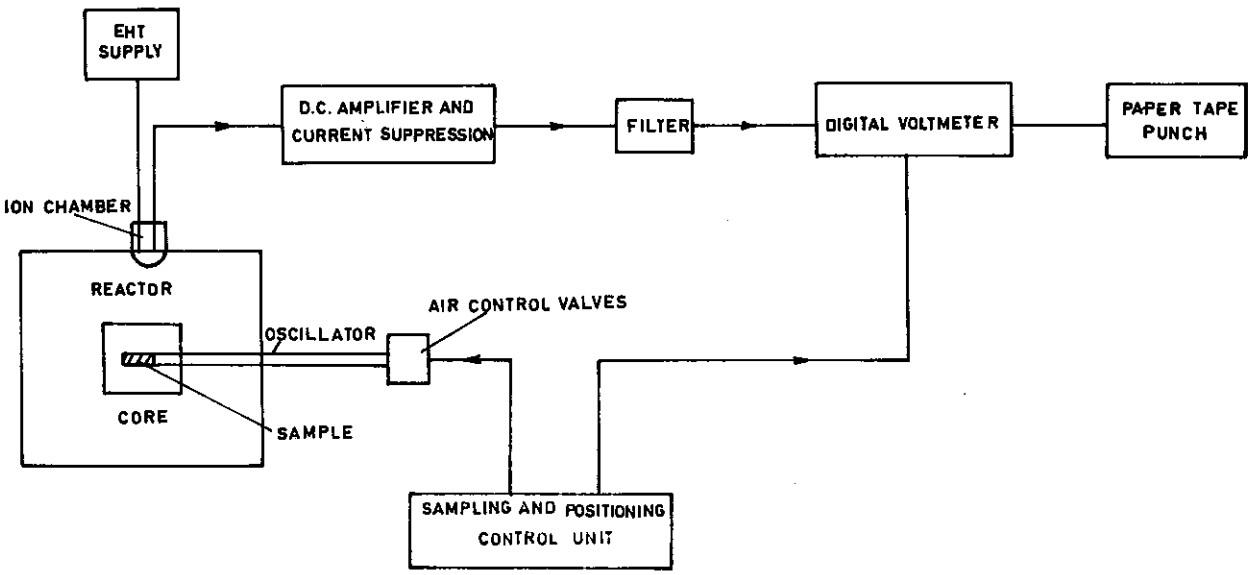

FIGURE 18. BLOCK DIAGRAM OF MOATA PNEUMATIC OSCILLATOR

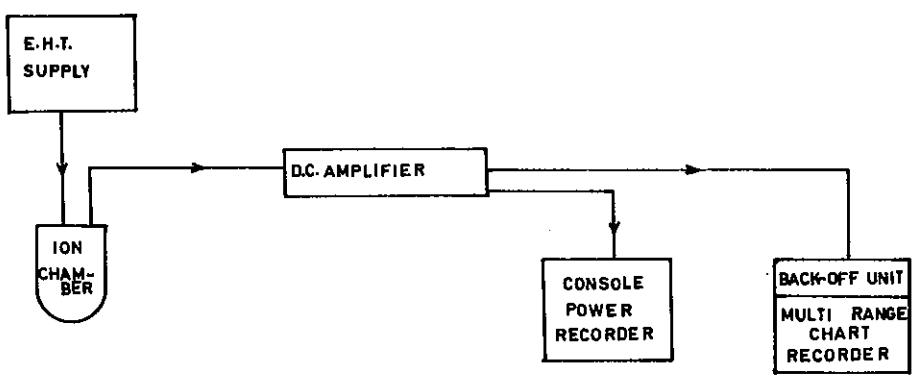

FIGURE 19. EXPANDED SCALE RECORDER EQUIPMENT

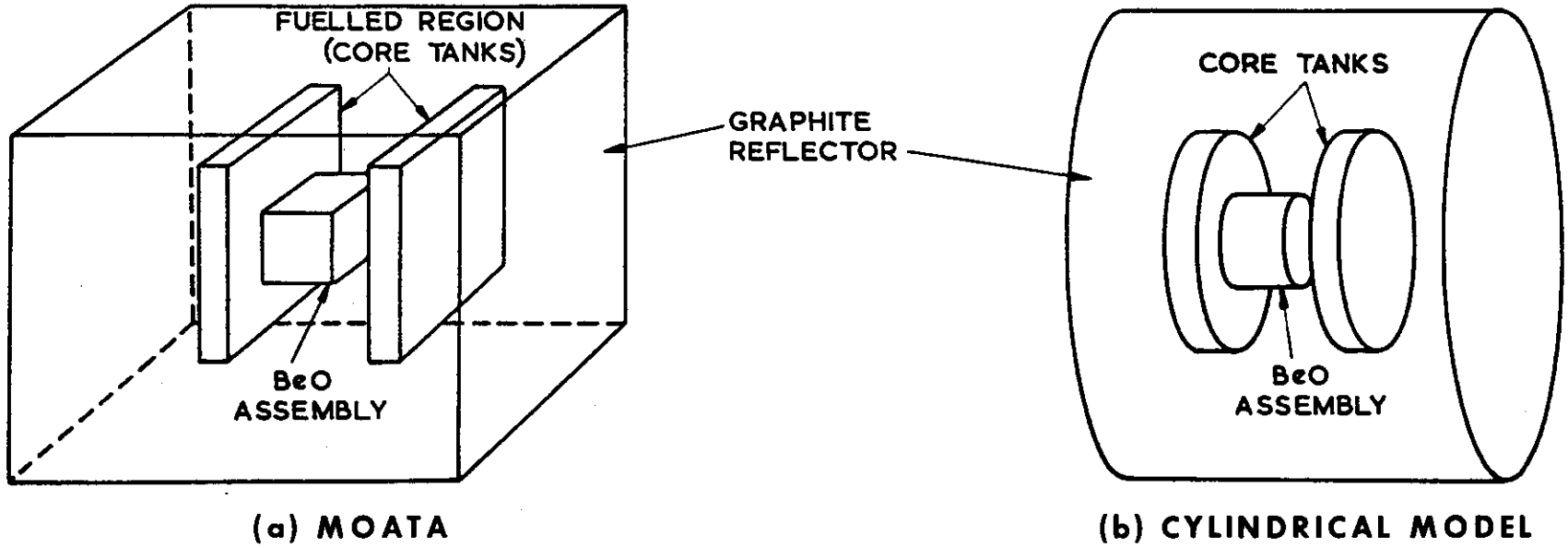

FIGURE 20. VIEW OF MOATA AND CYLINDRICAL MODEL FOR CRAM CALCULATIONS